AD-A135 987 MONOLITHIC ZNO SAW (SURFACE ACOUSTIC WAVES) STRUCTURES (U) PURDUE UNIV LAFAYETTE IN SCHOOL OF ELECTRICAL ENGINEERING R L GUNSHOR ET AL. 01 JUL 83 1/1

UNCLASSIFIED AFOSR-TR-83-1172 AFOSR-81-0214 F/G 9/5 NL

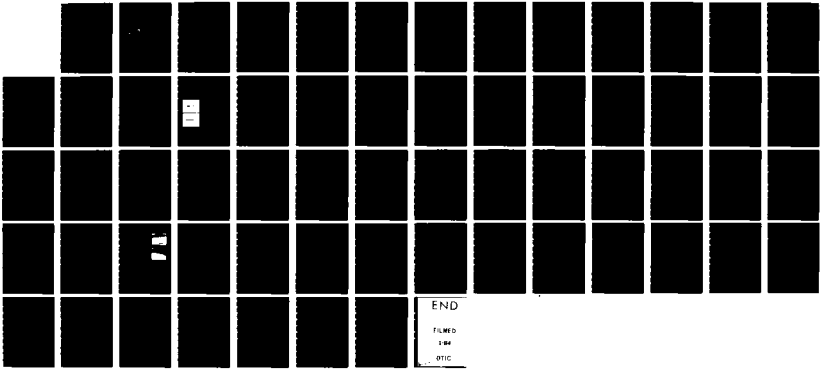

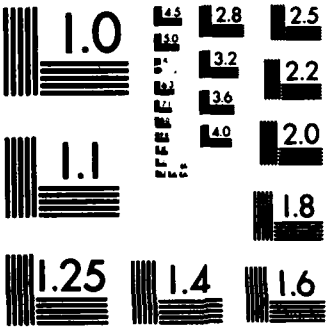

MICROCOPY RESOLUTION TEST CHART
NATIONAL BUREAU OF STANDARDS-1963-A

AFOSR-81-0214
Interim Scientific Report
1 July 1983

MONOLITHIC ZnO SAW STRUCTURES

R. L. Gunshor and R. F. Pierret

School of Electrical Engineering
Purdue University
West Lafayette, Indiana 47907

SECURITY CLASSIFICATION OF THIS PAGE (When Data Entered)

REPORT DOCUMENTATION PAGE		READ INSTRUCTIONS BEFORE COMPLETING FORM
1. REPORT NUMBER AFOSR-TR- 83-1172	2. GOVT ACCESSION NO. AD-A135	3. RECIPIENT'S CATALOG NUMBER 987
4. TITLE (and Subtitle) Monolithic ZnO SAW Structures		5. TYPE OF REPORT & PERIOD COVERED Interim Scientific Report 1 May 82 to 30 April 83
		6. PERFORMING ORG. REPORT NUMBER
7. AUTHOR(s) R. L. Gunshor and R. F. Pierret		8. CONTRACT OR GRANT NUMBER(s) AFOSR-81-0214
9. PERFORMING ORGANIZATION NAME AND ADDRESS School of Electrical Engineering Purdue University West Lafayette, IN 47907		10. PROGRAM ELEMENT, PROJECT, TASK AREA & WORK UNIT NUMBERS 61102F 2305/B1
11. CONTROLLING OFFICE NAME AND ADDRESS Air Force Office of Scientific Research/NE Building 410 Bolling AFB, D.C. 20332		12. REPORT DATE 1 July 83 13. NUMBER OF PAGES 60
14. MONITORING AGENCY NAME & ADDRESS(if different from Controlling Office)		15. SECURITY CLASS. (of this report) UNCLASSIFIED 15a. DECLASSIFICATION/DOWNGRADING SCHEDULE

16. DISTRIBUTION STATEMENT (of this Report)

Approved for public release; distribution unlimited.

17. DISTRIBUTION STATEMENT (of the abstract entered in Block 20, if different from Report)

18. SUPPLEMENTARY NOTES

N/A

19. KEY WORDS (Continue on reverse side if necessary and identify by block number)
Surface acoustic waves, ZnO, AlN piezoelectric devices, Microwave Acoustics, Electroacoustic convolvers, resonators

20. ABSTRACT (Continue on reverse side if necessary and identify by block number)
ZnO-on-silicon surface acoustic wave devices have been fabricated and tested. Electronic erasure of a stored correlator reference was demonstrated, the effect of laser annealing on propagation loss was examined, preliminary ageing studies were performed, and a conceptually new mode conversion resonator configuration was reported.

DD FORM 1473 EDITION OF 1 NOV 65 IS OBSOLETE UNCLASSIFIED

RESEARCH OBJECTIVES

Introduction

The role of monolithic surface acoustic wave (SAW) devices in performing the "real-time" analog of various signal processing functions is by now widely accepted. Monolithic structures are intrinsically rugged, reproducible, and compatable with modern integrated circuit fabrication techniques. The emphasis of the research reported herein involves the evaluation of monolithic SAW structures and materials, with the research treating in large part modified structures and prototype device concepts.

Specific Tasks

1. An important consideration in the ultimate application of SAW signal processing devices to real systems is the available bandwidth. As a consequence, a major aspect of the project involves measures aimed at increasing the available bandwidth of monolithic SAW devices.

2. ZnO has proven to be an acceptable piezoelectric material for the implementation of monolithic, "on-silicon" device concepts. An alternate material, AlN, has been proposed as representing a possible improvement over, and replacement for ZnO. A portion of the project has been devoted to an examination of AlN for monolithic SAW applications.

3. It has been established that the electrical properties of the Si-SiO_2 subsystem are adversely affected by the ZnO deposition process. Methods for minimizing the effects of the sputtering damage are being examined and evaluated. Also, an instability related to the injection of electrons from the metal gate electrode into the underlying ZnO is observed upon applying a d.c. gate bias. We are seeking an understanding and constructive control or blocking of this injection process.

4. A wide range of analog linear and nonlinear signal processing functions are now feasible as a result of continuing developments in acoustic surface wave techniques. Under investigation are problems associated with achieving practical devices, such as correlators and resonators, using the monolithic technology. A brief review of SAW devices on silicon is included as Appendix A.

A. Multilayer Structures-Bandwidth Considerations

A key consideration in the development of SAW materials and configurations is the matter of bandwidth. In dealing with layered media, some success has already been achieved as evidenced by the significant increase in bandwidth available to monolithic convolvers and correlators resulting from our demonstration of the advantage provided by use of the Sezawa mode for wave propagation. More recently we demonstrated the separate comb transducer, a development in the direction of increased operation frequency and bandwidth for monolithic devices.

The layered configuration under consideration is known to support a series of guided propagating modes. The lowest order of mode is called the Rayleigh mode; the next higher mode is named the Sezawa mode. Last year we reported experimental evidence of an efficient coupling between these two modes. A phase match between contrapropagating Rayleigh and Sezawa modes was obtained by employing an ion-milled array of grooves in the ZnO layer. Although these measurements were made in the context of developing an improved monolithic convolver configuration, it was found that a coneptually new resonator/filter was a direct result of mode coupling. Details of this development are found in the section of this report concerned with SAW resonator structures.

B. Charge Injection-Induced Junction Storage Correlator

Last year we reported a fabrication procedure for MZOS devices which resulted in the first bias-stable convolver. The stability was achieved through use of a particular annealing procedure. All previously reported MZOS convolvers and correlators exhibit the bias instability.

In contrast to efforts directed at stabilizing the MZOS configuration, the bias instability in question, resulting from injected charge at a gate electrode, has been employed in a new storage correlator configuration which we reported last year. The new device concept utilizes charge stored in deep states at the ZnO-SiO_2 interface to induce discrete, isolated, inverted regions at the silicon surface. The resulting MOS diode regions perform the task of information storage, and serve as replacement for pn and Schottky diode arrays employed in previously proposed storage configurations. The advantage here is a significantly reduced fabrication complexity.

Most recently, we have reported an additional feature of the induced junction correlator, that of electronic erasure of the stored reference. Last year we speculated that electronic erasure of a stored signal could be readily implemented with an induced junction correlator. Details of the ease with which the stored signal can be erased, and the resulting availability for storage of a new reference signal, is described in Appendix B.

A new configuration for the induced junction correlator, expected to exhibit improved characteristics, is currently under study.

C. SAW Resonators on Silicon

During the past year we have examined several aspects of the performance of our previously reported (A complete discussion of SAW resonators on silicon is included in the reprint of Appendix C.) on-silicon resonators; in addition a conceptually new resonant structure based on mode conversion has been developed.

One study concerned a preliminary examination of the ageing characteristics of the temperature stable $ZnO/SiO_2/Si$ resonator. Automated measurements performed on several resonators by E. Staples at North American Rockwell revealed a degree of stability comparable to a control group of quartz resonators. The time involved was several weeks, so only preliminary conclusions are possible. Results of these measurements were reported, and are included as reprints in Appendix A and D.

Recently reported experiments have demonstrated an improvement in optical loss in ZnO guiding films resulting from a laser annealing procedure. We have subsequently performed CO_2 laser annealing experiments to determine the effect on acoustic propagation loss.

It is believed that the dominant loss mechanisms for a properly fabricated $ZnO/SiO_2/Si$ VHF or UHF resonator is associated with propagation loss in the ZnO layer. We had, in fact, proposed that resonator Q is a sensitive measure of propagation loss. (Propagation loss is an important, and often controversial measure of ZnO film quality.) The results of our laser annealing experiments were evaluated by measurement of resonator Q and center frequency. It was found that the relatively small reduction in acoustic loss was reflected in an increase of resonator Q. Since it is thought that the anneal primarily affects the ZnO/SiO_2 interface, the improvement in Q is expected to become increasingly significant as resonators are constructed for higher frequencies.

Details of the laser annealing experiment were reported at the Frequency Control Symposium (Appendix E).

The operation of the mode conversion resonator, a conceptually new device based on the propagation of surface acoustic waves in layered structures, was reported this year. Both Rayleigh and Sezawa modes propagate when the ZnO layer is sufficiently thick. By employing a periodic array of milled grooves, it is possible to couple (phase match) modes propagating in opposite directions, the result is a mode conversion "reflector". A resonator has been constructed in which input and output transducers are bracketed by a pair of such arrays. Mode conversion resonator Q values of 3000 have been measured, indicating an extremely high mode-to-mode conversion efficiency. The advantage of a mode conversion resonator over one using Bragg reflctors lies in the reduction of direct acoustic coupling between input and output transducers, as each is optimized for coupling to a different mode. (Input and output transducers are fabricated with different element perrodicity.) Details of this work are found in reprints/preprints in Appendix D, E, and F.

During the past year we performed experiments designed to explore the feasibility of using $ZnO/SiO_2/Si$ resonators as the basis of an accelerometer, with applications, for example, to aircraft navigation. We fabricated a cantilever mounted resonator for sensing force. It was found that the frequency of the VHF resonator varied linearly with applied force up to the fracture point of silicon. From the results of these experiments, one could envision a device exhibiting a dynamic range of 10^5. Details are given in the reprint found in Appendix G.

D. ZnO Film Properties

A recent development is the completion of a study comparing the properties of rf diode and magnetron sputtered ZnO-SiO_2-Si structures. A major impetus for the comparative evaluation was the previously described achievement of bias stability in annealed magnetron-sputtered films but not in similarly processed diode-sputtered films. The comparison incorporated both electrical data and physical data derived from SEM, X-ray diffraction, and other analytical techniques. The interfacial trap and net effective charge densities at the Si-SiO_2 interface, ZnO film morphology, ZnO film conductance, and the electrical and physical effects of post-deposition annealing were among the topics addressed in the comparison. One interesting result of the work was the observation that radiation damage produced in the underlying Si-SiO_2 subsystem during sputtering of the ZnO film was a function of the substrate positioning on the

sputtering platform, with the spatial dependence being especially pronounced for magnetron sputtering. Magnetron films were also found to have a coarser fiber morphology. It was generally concluded from the data that the magnetron films contained a much higher density of upper band gap traps whose numbers were increased by annealing. It is our belief that these traps play the key role in the bias stability of annealed magnetron devices and arise as a direct consequence of the large fiber morphology of the magnetron films. A reprint describing these results is included in Appendix H.

E. New Materials

The recent acquisition of an MBE facility has led us to examine the possibility of new materials/configurations. During the past year we have theoretically examined the device implications of the propagation of an acoustic plasma mode in a multi-layered structure. It is found that the existence of such modes in the 500 GHz range is feasible, although the design of a suitable transducer appears difficult. Details of the analysis are given in the preprint of Appendix I.

PUBLICATIONS

S. J. Martin, S. S. Schwartz, R. L. Gunshor, and R. F. Pierret, "Surface Acoustic Wave Resonators on a ZnO-on-Si Layered Medium," Journal of Applied Physics, 54, 561 (1983).

R. L. Gunshor, S. J. Martin, and R. F. Pierret, "Surface Acoustic Wave Devices on Silicon" (Invited), presented at Conference on Solid State Devices, Tokyo, August 1982.

K. C. Weng, R. L. Gunshor, R. F. Pierret, and K. Tsubouchi, "Electronic Erasure of Stored Reference Signals in a Metal-ZnO-SiO_2-Si Induced Junction Storage Correlator," Electronics Letters 18, 1078 (1982).

S. J. Martin, S. Datta, R. L. Gunshor, R. F. Pierret, M. R. Melloch, and E. J. Staples, "SAW Resonators on Silicon," presented at 1982 IEEE Ultrasonics Symposium, San Diego, October 1982.

S. J. Martin, R. L. Gunshor, T. J. Miller, S. Datta, R. F. Pierret, and M. R. Melloch, "Surface Wave Resonators on Silicon," paper presented at the Frequency Control Symposium, Philadelphia, June 1982.

S. J. Martin, R. L. Gunshor, M. R. Melloch, S. Datta, and R. F. Pierret, "Surface Acoustic Wave Mode Conversion Resonator," Applied Physics Letters 43, 238 (1983).

S. J. Martin, R. L. Gunshor, R. F. Pierret, and G. Gorodetsky, "Uniaxially Strained ZnO/SiO_2/Si SAW Resonators," Electronics Letters 18, 1030 (1982).

R. D. Cherne, R. F. Pierret, and R. L. Gunshor, "Comparative Evaluation of rf Diode and Magnetron Sputtered ZnO-SiO_2-Si Structures," paper presented at 1982 IEEE Ultrasonics Symposium, San Diego, October 1982.

S. Datta and R. L. Gunshor, "Space Charge Waves in Multilayered Heterostructures," paper to be published in the Journal of Applied Physics, 1983.

PERSONNEL

Robert L. Gunshor, Professor of Electrical Engineering

Robert F. Pierret, Professor of Electrical Engineering

Supriyo Datta, Assistant Professor of Electrical Engineering

Ken Weng, Graduate Research Assistant

Steve J. Martin, Graduate Research Assistant

Larry Pearce, Graduate Research Assistant

Jeff A. Shields, Graduate Research Assistant

Mike Church, Graduate Research Assistant

Supriyo Bandyopadhyay, Graduate Research Assistant

Tim Miller, Technician

Proceedings of the 14th Conference (1982 International) on Solid State Devices, Tokyo, 1982;
Japanese Journal of Applied Physics, Volume 22 (1983) Supplement 22-1, pp. 37-41

(Invited) Surface Acoustic Wave Devices on Silicon

R. L. GUNSHOR, S. J. MARTIN and R. F. PIERRET

School of Electrical Engineering, Purdue University,
West Lafayette, IN 47907, U.S.A.

Surface acoustic wave (SAW) devices can be used to perform a number of real-time signal processing functions. Originally, SAW devices were constructed on single-crystal piezoelectric materials such as $LiNbO_3$ and quartz. In this paper we discuss the manner in which several SAW devices can be implemented on non-piezoelectric silicon substrates, thereby facilitating their use in integrated circuits. The pn diode memory correlator and the SAW resonator are discussed in detail. The $ZnO/SiO_2/Si$ layered medium can be made temperature stable by controlling the thermal SiO_2 thickness. This, together with new ageing data, demonstrates the practicality of including SAW devices in monolithic integrated circuits.

§1. Introduction

For many years bulk-wave acoustic devices were used in electronic systems to perform various signal processing functions. With the discovery of an efficient means of electrical to acoustic transduction around 1965 [1], surface acoustic wave (SAW) devices have produced a resurgence of interest in acoustic waves in electronics. The existence of a propagating acoustic mode which is confined by the waveguiding nature of a surface makes possible planar acoustic devices. The use of a piezoelectric substrate, in which mechanical displacement is coupled to electric field, permits the efficient excitation of the surface wave by means of an interdigital transducer (IDT). In addition to efficient transduction, the planar nature of SAW devices is advantageous for other reasons. Not only is the wave accessible along its path for modification or sampling, but also SAW devices are potentially compatible with integrated circuit technology.

In order to be IC integrable, or to take advantage of other semiconductor properties, a technology has evolved for fabricating several SAW devices on silicon substrates. The first device to be discussed, a SAW storage correlator, relies on an interaction between acoustoelectric fields and charge carriers in the silicon substrate. The need for IC components with good UHF performance, such as in high-Q tuned circuits, provides the motivation for building SAW resonators on silicon, the second device to be discussed. To implement SAW devices on the non-piezoelectric silicon substrate it is necessary to incorporate a piezoelectric film such as ZnO or AlN. These films are typically deposited onto the silicon by RF or diode sputtering [2] or by chemical vapor deposition. The electromechanical coupling provided by the piezoelectric film varies with film thickness, dictating a film thickness to acoustic wavelength ratio h/λ of between 0.05 and 0.5.

§2. $ZnO/SiO_2/Si$ Storage Correlator

The main signal processing task of SAW convolvers or correlators is to serve as analog to the mathematical functions for which they are named. These non-linear signal processing tasks can be performed electronically by digital and CCD circuits, with each competing technique having its advantages and disadvantages. The digital techniques of today are not fast enough for certain broadband applications and are relatively expensive; charge-coupled devices and presently most widely applied for bandwidths less than 10 MHz. Where real-time, wideband (10 to 300 MHz) performance is desired, SAW devices provide an alternative.

Convolution is accomplished with surface waves by applying two modulated signals, $V_1(t)$ and $V_2(t)$ of a common carrier frequency to two IDT's separated by a gate electrode, as shown in Fig. 1. The electric fields accompanying the counterpropagating waves are multiplied through a nonlinear interaction with chargecarriers in the semiconductor [3] and are summed over the interaction region by means of the intervening gate electrode. [4] The

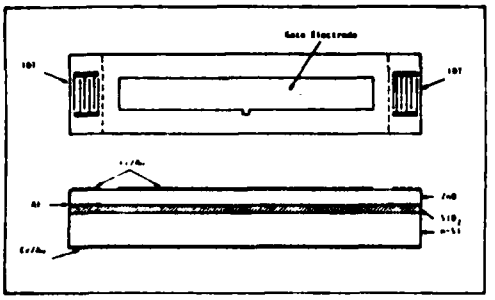

Fig. 1. ZnO-on-Si SAW convolver device configuration.

envelope of the output signal, $V_3(t)$, taken from the gate electrode, is the convolution of the two input signals, following the prescription:

$$V_3(t) = A \int V_1(\tau) V_2(t-\tau)\, d\tau \qquad (1)$$

If $V_2(t)$ is a time-inverted form of $V_1(t)$, the output is then the autocorrelation of $V_1(t)$ with the convolver functioning as a matched filter. In radar applications, where good time resolution as well as the elimination of interfering signals is important, the delay time/bandwidth product is the figure of merit. As the return time of the interrogating pulse is unknown *a priori*, it is advantageous to incorporate storage capability for the reference signal. This is the so-called storage correlator. Several schemes have been devised for signal storage, all involving properties of the semiconductor substrate. The reference signal memory function has been achieved using the storage of reference-related charge in Si–SiO_2 interface states [5], Schottky diodes [6], pn diodes [7, 8], and most recently in isolated induced-junction arrays [9].

Herein we describe a recently reported pn diode storage correlator, the configuration of which is shown in Fig. 2. An RF reference signal to be stored is applied to the gate (ω, $k=0$) in coincidence with a narrow acoustic pulse (ω, k) propagating under the gate. The simultaneous presence at the silicon surface of the RF reference signal and the electric field associated with the acoustic signal produces a resultant electric field component normal to the silicon surface. This electric field component, arising from a nonlinear interaction between the reference signal and the narrow acoustic pulse, serves to inject charge into the diodes. The result is that a spatially varying charge pattern ($\omega=0, k$), representing the sampled reference signal, is maintained in the diode array. The signal storage time, limited by diode leakage current, is typically tens of milliseconds to a few seconds.

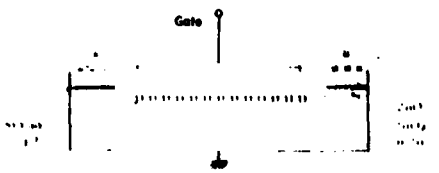

Fig. 2. SAW memory correlator on silicon utilizing pn diode array for reference signal storage.

Upon arrival of the interrogating signal, it is applied to the gate electrode. Because of the nonlinear interaction of the interrogating SAW ($\omega, k=0$) with the stored charge pattern ($\omega=0, k$), a correlation output (ω, k) is detected at an IDT. ZnO-on-silicon monolithic convolvers and storage correlators have been operated at frequencies up to 355 MHz [10], with fractional bandwidths of up to 20%[11]. Device efficiencies (P_{out}(dBm) − P_{in1}(dBm) − P_{in2}(dBm)) of −53 dBm have been achieved in convolvers, with −66 dBm for memory correlators.

§3. VHF-UHF Resonators on Silicon

The second class of SAW devices fabricated on silicon, the SAW resonator, does not involve the electronic properties of the semiconductor. By converting an electromagnetic signal into an acoustic wave, the SAW resonator utilizes acoustic resonance to form high-Q reactive elements for filters, tuned circuits, and to perform frequency control functions. Wideband integrated circuits are readily implemented with film capacitors and active devices as inductors however, such circuits are characterized by low Q values.

The SAW resonator is formed by creating a resonant cavity between two distributed Bragg reflectors. These distributed reflectors are formed by perturbing the acoustic propagation path at half-wavelength intervals with metal strip overlays [12], or with grooves etched in the surface [13]. Each feature reflects approximately 1% of the incident wave amplitude, so that the array produces strong coherent

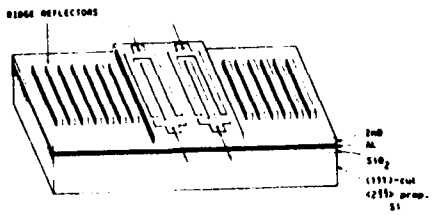

Fig. 3. ZnO-on-Si SAW two-port resonator with etched groove reflectior arrays. Typically 400 grooves per reflector array and 8 finger-pair IDTs are used.

reflection within a narrow frequency range. In addition to minimizing the surface wave conversion to bulk modes, the distributed reflection scheme—by virtue of its narrow bandwidth—permits single mode resonators to be constructed. The best resonator performance to date has been achieved with grooves formed by ion beam etching of the ZnO surface, as shown in Fig. 3.

Energy is coupled into and out of the SAW resonant cavity by means of one or two interdigital transducers placed such that fingers lie at the maxima of the standing wave potential. Two-port resonators function as narrow band filters, while single port devices serve as high-Q reactive elements. The transfer characteristics of a two-port device, as measured on a network analyzer, is shown in Fig. 4. SAW resonators on silicon exhibit Q values in the 3,000 to 12,000 range near 100 MHz. Q-values are limited by propagation loss, which is believed to originate predominantly in the ZnO film. In fact, the Q measurement is a useful technique for evaluating propagation loss.

Applications requiring a high-Q filter or reactive element generally require stability over time and temperature. Temperature will influence resonant frequency if either the dimension of the medium in the direction of propagation is changed or the phase velocity is changed. Typically resonators exhibit a parabolic fluctuation in resonant frequency with temperature. The standard for temperature stability is set by resonators fabricated on the ST cut of quartz. These devices show a turn-over temperature—the point where the derivative is zero—near 20°C, with a second order temperature coefficient of frequency of -0.0315 ppm/(degC)^2.

The ZnO-on-Si medium does not exhibit the extraordinary temperature stability of ST-quartz at room temperature. The turn-over temperature lies well below room temperature so that a 25 ppm/(degC) decrease in resonant frequency is measured at 20°C. It is found, however, that the presence of a thermally grown silicon dioxide layer between the silicon substrate and the ZnO layer serves to increase the turnover temperature in proportion to SiO_2 thickness. Consequently, when SiO_2 thickness is 0.076 λ_0, where λ_0 is the resonant SAW wavelength, the turn-over temperature occurs at room temperature and displays a second order temperature coefficient of -0.052 ppm/(degC)^2. This ability to temperature compensate the ZnO/Si medium with SiO_2 is due to the opposing sign of the temperature coefficient of stiffness.

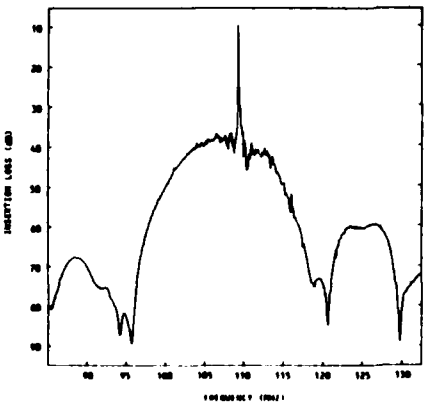

Fig. 4. Insertion loss measured between transducers of a two-port SAW resonator vs frequency. At resonance, the transmission is enhanced 28 dB over the delay-line response.

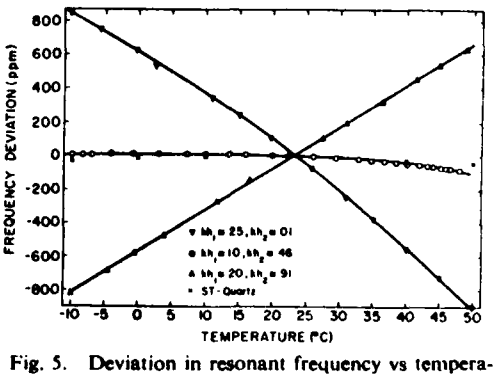

Fig. 5. Deviation in resonant frequency vs temperature for several ZnO/SiO_2/Si layer configurations. kh_1 denotes ZnO thickness, kh_2 denotes SiO_2 thickness, both normalized to acoustic wavelength.

Compensation provides temperature stability comparable to that of ST-quartz, with the option of elevating the turn-over temperature for use in an oven-maintained environment. In Fig. 5, the drift in resonant frequency with temperature is shown for several values of SiO_2 thickness. Data for devices built on ST-quartz are shown for comparison [14]. It should be noted that the temperature compensating SiO_2 thickness quoted is for a (111)-cut Si substrate and seems to be relatively independent of the thin ZnO layers typically used.

With regard to resonator stability over time, an initial ageing study has been performed. After a 24 hour vacuum bakeout at 125°C, five ZnO-on-Si resonators were hermetically packaged. The devices were not fixed to the header in order to eliminate possible age-inducing stresses. The resonant frequency of each port of the five two-port devices was monitored over a several-week period as shown in Fig. 6. All of the devices exhibited a rapid increase in frequency of from 15 to 50 ppm over the first 24 hours; the cause of this initial jump in frequency is unknown. The subsequent gradual decline in resonant frequency observed for some devices is characteristic of a failure to achieve a hermetic seal in device packaging. Two of the devices, however, displayed promising ageing characteristics, drifting less than 10 ppm during the subsequent ageing period. The temperature characteristics and ageing behavior of SAW resonators, it should be added, may possibly be influenced by mounting and bonding methods.

§4. Conclusion and Acknowledgements

The most recent generation of SAW devices

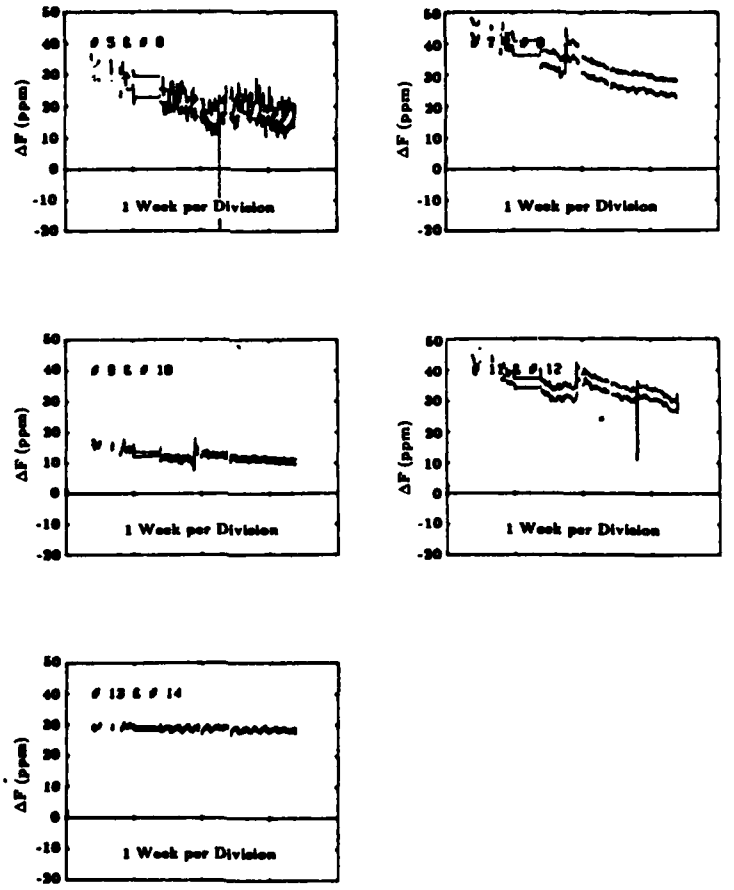

Fig. 6. Aging characteristics of ZnO-on-Si SAW resonators. The two traces in each plot represent deviation in resonant frequency for each of the two resonator ports.

are fabricated on semiconductor wafers to form monolithic circuits. Although both silicon and gallium arsenide substrates have been used, this paper emphasizes Si devices as the majority candidate. The $ZnO/SiO_2/Si$ device configuration comes closest to the initial SAW promise for compatability with conventional IC technology.

The authors wish to thank Dr. E. J. Staples of North American Rockwell Corporation for performing the ageing test, and Gary McGee of the Naval Avionics Center for help in making photomasks. The work was supported by the Air Force Office of Scientific Research, the National Science Foundation, and the NSF-MRL program.

References

1) R. M. White and F. W. Voltmer: Appl. Phys. Lett. **7** (1965) 314.
2) F. S. Hickernell: **1980** *Ultrasonics Symposium Proceedings, Boston* (IEEE, New York, 1980) p. 785.
3) R. L. Gunshor: *Solid State Electron.* **18** (1975) 1089.
4) K. Tsubouchi, S. Minagawa and N. Mikoshiba: J. Appl. Phys. **47** (1976) 5187.
5) A. Bers and J. H. Cafarella: Appl. Phys. Lett. **25** (1974) 133.
6) K. A. Ingebrigtsen: *Proc. IEEE* **64** (1976) p. 674.
7) H. C. Tuan and G. S. Kino: Appl. Phys. Lett. **31** (1977) 641.
8) F. C. Lo, R. L. Gunshor and R. F. Pierret: Appl. Phys. Lett. **34** (1979) 725.
9) K. C. K. Weng, R. L. Gunshor and R. F. Pierret: Appl. Phys. Lett. **40** (1982) 71.
10) M. R. Melloch, R. L. Gunshor and R. F. Pierret: Electron. Lett. **17** (1981) 827.
11) J. E. Bowers, B. T. Khuri-Yakub and G. S. Kino: Appl. Phys. Lett. **36** (1980) 806.
12) S. J. Martin, R. L. Gunshor and R. F. Pierret: Appl. Phys. Lett. **37** (1980) 700.
13) S. J. Martin, R. L. Gunshor and R. F. Pierret: **1980** *Ultrasonics Symposium Proceedings, Boston* (IEEE, New York, 1980) p. 113.
14) D. Hauden, M. Michel, G. Bardeche and J. J. Gagnepain: Appl. Phys. Lett. **31** (1977) 315.

APPENDIX B

ELECTRONIC ERASURE OF STORED REFERENCE SIGNALS IN A METAL-ZnO-SiO_2-Si INDUCED JUNCTION STORAGE CORRELATOR

Indexing terms: Semiconductor devices and materials, Surface-acoustic-wave devices, Signal erasure

The surface-acoustic-wave storage correlator is used to store a reference signal for subsequent correlation with an unknown signal. We describe and demonstrate a method for the electronic erasure of stored signals in the context of the MZOS-induced junction storage correlator.

The ability of surface-acoustic-wave (SAW) devices to perform nonlinear signal processing functions such as convolution and correlation is enhanced by incorporating a reference signal storage capability into the device. Several SAW correlator device configurations have been described in which the storage correlation operation is achieved through the storage of a reference signal as a spatially varying charge pattern at the silicon surface. Within the storage time limitation of the particular storage mechanism (surface states,[1] Schottky diodes,[2] *pn* diodes[3,4] or an array of induced junctions[5]), the stored signal can be correlated with an 'unknown' input signal by employing a nonlinear interaction between the signal and the stored charge pattern. In many envisioned signal processing applications it would be desirable to have the capability of rapidly erasing and replacing the stored reference signal. Removal of the stored signal in a SAW storage correlator has been previously demonstrated for an array of Schottky diodes;[6] there the diodes were illuminated by an LED with an appropriate output wavelength. In this letter we describe and demonstrate a new method of stored signal erasure, electronic erasure, implemented with the induced junction ZnO-on-Si storage correlator.[5]

The schematic of the induced junction storage correlator employed in the electronic erasure experiment is shown in Fig. 1. The key feature of an induced junction device is the incorporation of an aluminium grating at the ZnO-SiO_2 interface. When a negative bias is applied to the gate of an MZOS correlator, electrons are injected into the ZnO film and are subsequently trapped at or near the ZnO-SiO_2 interface. This same phenomenon is known to cause the major bias instability associated with MZOS SAW devices.[7] However, with the introduction of a metal grating, the charge injection phenomenon can be used constructively to create signal storage regions beneath the silicon surface. Under operational conditions, inversion regions of minority carrier storage at the silicon surface are separated by depleted or slightly accumulated regions under the aluminium strips. The reference signal is stored as a result of the interaction between the reference signal applied to the gate and a narrow acoustic pulse propagating under the gate. The electric fields resulting from this interaction produce a nonequilibrium minority-carrier charge density (a charge deficit) within the inversion regions; this deficit constitutes the signal storage. Storage times of up to 80 ms (corresponding to a 3 dB decrease in output) have been achieved in prototype devices.

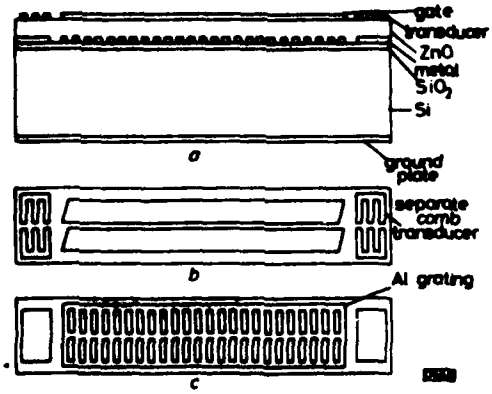

Fig. 1 *Induced junction storage correlator*
a Cross-section of device
b Top metallisation
c Interface Al grating

Electronic erasure of the storage signal is achieved by creating shunting paths between the induced junctions while simultaneously promoting the lateral flow of minority carriers between these regions and the inverted area surrounding the gate. The shunting paths which result in the loss of the stored signal are produced through the application of a sufficiently large negative DC pulse to the gate. On application of such a pulse, electrons are injected into the ZnO and rapidly collect on the Al grating. The silicon surface under the Al grating responds to this pulse by being forced into deep depletion. (Deep depletion is a nonequilibrium condition inside the silicon where the depletion region is extended deeper into the bulk than the maximum width at thermal equilibrium.) Because the surface potential beneath the grating is lower than surrounding regions, minority carriers originally in the induced junctions and the area lateral to the gate now migrate into the grating region, thereby tending to establish a more or less uniform distribution of minority carriers throughout the structure. The envisioned carrier motion is very similar to that in charge-coupled devices. It should be noted that the inversion layer lateral to the gate is established during the initiation procedure which produces the induced junction. Owing to high lateral conductivity at the ZnO surface, electrons are injected into the ZnO-SiO_2 interface outside the delay line and drive the silicon surface surrounding the induced junction array into inversion. It is these inversion layer charges which move laterally into the gated area.

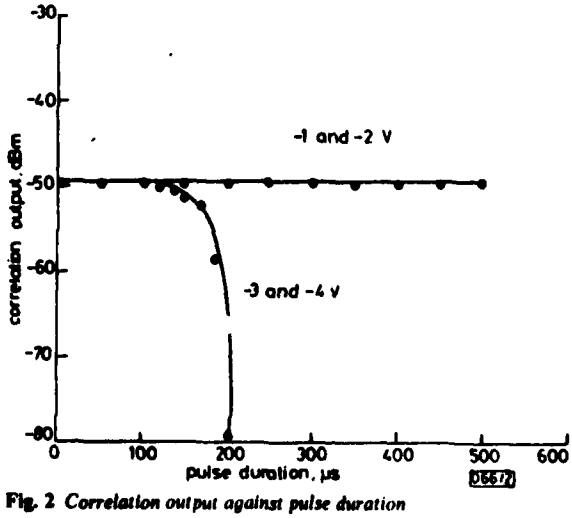

Fig. 2 *Correlation output against pulse duration*

In performing the signal erasure experiment, applied negative DC pulses of different amplitudes and durations were applied to the gate within the signal storage time. The results of this experiment are shown in Fig. 2. For the given device structure and a gate pulse bias more positive than $-2{\cdot}5$ V, no signal erasure was observed. The reference signal was completely erased, however, with pulses more negative than $-2{\cdot}75$ V and having durations longer than 200 μs. Since thermal generation in the near-surface region is relatively slow, it cannot account for the short 200 μs time for erasure. The formation of a shunting path under the grating is clearly controlled by the lateral flow of minority carriers. Fig. 3 illustrates the erasure of a stored signal with a -3 V, 200 μs pulse. The upper trace shows the output without an erasure pulse, while output following a negative erasure pulse is shown in the lower trace. (The small residual pulse in the lower trace is a spurious signal from the measurement set-up, and can also be seen at end of the output signal in the upper trace.)

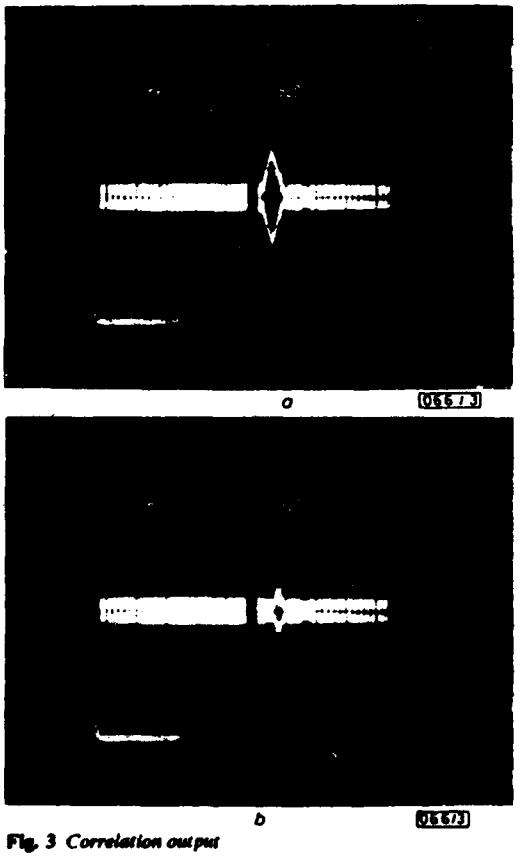

Fig. 3 *Correlation output*
a Without erasure pulse
b With erasure pulse

After application of the erasure pulse and subsequent return of the gate bias to zero volts, injected electrons located on the Al grating are rapidly withdrawn from the interior of the structure. The excess minority carriers beneath the Al grating are in turn annihilated through recombination and possibly lateral motion to regions surrounding the gate. In other words the shunting path under the Al grating is thereby removed, returning the device to a condition where an array of isolated minority-carrier storage regions are ready for the storage of a fresh reference signal. Experimentally, by varying the time interval between the erasure pulse and the following writing pulse, we have observed that at least 400 μs is needed before a new signal can be stored.

In conclusion, we have described and demonstrated a new method for electrically erasing the stored signal in an induced junction storage correlator. The electronic erasure method may be useful in signal processing applications where ready replacement of the stored reference signal is required.

The authors thank S. Phillips and G. Magee of the Naval Avionics Facility for photomasks. The research was supported by AFOSR grant ~~AF-810214~~ AFOSR-81-0214 and NSF grant ECS 8009793.

K. C.-K. WENG
R. L. GUNSHOR
R. F. PIERRET
K. TSUBOUCHI*

School of Electrical Engineering
Purdue University
West Lafayette, IN 47907, USA

* On leave from Research Institute of Electrical Communication, Tohoku University, Japan

19th October 1982

References

1 BERS, A., and CAFARELLA, J. H.: 'Surface state memory in surface acoustoelectric correlator', *Appl. Phys. Lett.*, 1974, **25**, pp. 133–135

2 INGEBRIGTSEN, K. A., COHEN, R. A., and MOUNTAIN, R. W.: 'A Schottky diode acoustic memory and correlators', *ibid.*, 1975, **26**, pp. 596–598

3 LO, F. C., GUNSHOR, R. L., and PIERRET, R. F.: 'Monolithic (ZnO) Sezawa mode *pn*-diode-array memory correlator', *ibid.*, 1979, **34**, pp. 725–726

4 TUAN, H. C., KHURI-YAKUB, B. T., and KINO, G. S.: 'A monolithic zinc-oxide-on-silicon *pn*-diode storage correlator', *ibid.*, 1977, **31**, pp. 641–643

5 WENG, K. C.-K., GUNSHOR, R. L., and PIERRET, R. F.: 'Induced junction monolithic zinc oxide-on-silicon storage correlator', *ibid.*, 1982, **40**, pp. 71–73

6 RALSTON, R. W., and CAFARELLA, J. H.: 'Improved acoustoelectric Schottky-diode/$LiNbO_3$ memory correlator'. 1977 Ultrasonics Symposium Proceedings, IEEE cat. no. 77CH1264-ISU, pp. 472–477

7 PIERRET, R. F., GUNSHOR, R. L., and CORNELL, M. E.: 'Charge injection in metal-ZnO-SiO_2-Si structures', *J. Appl. Phys.*, 1979, **50**, pp. 8112–8124

0013-5194/82/251078-03$1.50/0

Surface acoustic wave resonators on a ZnO-on-Si layered medium

S. J. Martin, S. S. Schwartz, R. L. Gunshor, and R. F. Pierret
School of Electrical Engineering, Purdue University, West Lafayette, Indiana 47907

(Received 22 March 1982; accepted for publication 5 October 1982)

The adaptation of surface acoustic wave resonator technology to a ZnO-on-Si layered medium is presented. Several distributed reflector schemes are considered, including shorted and isolated metallic strips, as well as grooves etched in the ZnO layer. In the case of etched groove reflectors, a first-order velocity perturbation arises due to the dispersive nature of the layered medium. Unique resonator design considerations result from the reflector array velocity and reflectivity characteristics. Transverse mode resonances are characterized and their effect on resonator response eliminated by a novel transducer design. A technique for temperature compensating the devices by use of a thermal SiO_2 layer is discussed.

PACS numbers: 43.35.Pt, 62.40. + i, 84.30.Vn, 85.40. – e

I. INTRODUCTION

The surface acoustic wave (SAW) resonator has been developed over the past decade into a practical means for achieving narrow-band frequency filtering in the VHF to UHF range. Devices having resonant frequencies in the range 20–2600 MHz perform the tasks which fundamental bulk wave resonators perform below 20 MHz. Applications for such devices include frequency control functions in oscillators, for which the narrow bandwidth and high rejection of off-resonant frequencies ensure precise frequency selectivity and spectral purity. Also used as tuned circuits, SAW resonators have recently been applied for clock recovery in digital PCM regenerators.[1] Heretofore, SAW resonators have been built almost exclusively on single crystal piezoelectric substrates. As examples, lithium niobate is atrractive for its high value of electromechanical coupling, while temperature stability favors ST-quartz. This paper is an expansion of earlier reports on the adaptation of SAW resonator technology to a ZnO-on-Si layered medium.[2,3] The motivation for using silicon as a substrate lies in the possibility of incorporating the SAW resonator in monolithic integrated circuits, thereby eliminating the need for off-chip components as are presently required in the single-crystal embodiments.

In the next section we discuss the fabrication of the ZnO-on-Si SAW resonator. Sections III and IV are devoted to analyzing metal grating and etched groove distributed reflectors. The unusual characteristics of the etched groove reflector lead to unique design considerations with regard to transducer positioning and apodization, presented in Secs. V and VI. Finally, temperature stabilization is considered in Sec. VII.

II. BASIC DEVICE STRUCTURE

The two-port SAW resonator consists of separate input and output interdigital transducers positioned inside a resonant cavity formed by two distributed reflectors.[4,5] Figure 1 shows the basic ZnO-on-Si device structure. Like the SAW resonators built on single crystal substrates, the ZnO-on-Si version is a planar device with acoustic energy confined to within roughly one acoustic wavelength of the surface. In contrast to the Rayleigh distribution of acoustic amplitude found in a semi-infinite half-space, however, the added boundary conditions imposed at the interfaces between layers govern the distribution of wave amplitude in the surface-normal direction.[6] This dependence of wave distribution on layer properties is reflected in the values of electromechanical coupling and surface wave velocity, as well as the wave reflectivity arising from perturbing features on top of the ZnO. Consequently, the disposition of surface features, intended to transduce or reflect acoustic waves, is highly dependent on the layer configuration forming the acoustic medium. By "layer configuration", we mean the combination of substrate orientation, together with layer thicknesses and electrical boundary conditions imposed by conductive shorting planes which determine the acoustic and electrical characteristics of the medium. The ZnO and SiO_2 layer thicknesses, normalized to wavenumber, are denoted by h_1k, h_2k, respectively, while for acoustic purposes the aluminum shorting plane, shown in Fig. 1, is regarded as vanishingly thin. It is apparent that there are a large number of variables in the layered acoustic medium; practical considerations will tend to provide limits.

In fabricating the devices, both (100) and (111) cuts of silicon have been used as substrates, with wave propagation along the $\langle 010 \rangle$ and $\langle \bar{2}11 \rangle$ directions, respectively. These pure mode directions result in a decoupling of the transverse mode from the Rayleigh-like mode, permitting selective excitation of the latter by means of an interdigital transducer (IDT). The essential purpose of the SiO_2 layer is to provide

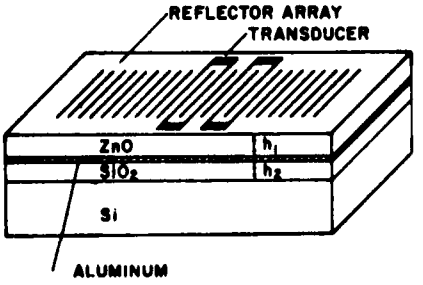

FIG. 1. Surface acoustic wave two-port resonator using piezoelectric ZnO layer on thermally oxidized Si substrate. An aluminum shorting plane is included to enhance transduction as well as shielding carriers in the substrate from electric fields.

 0021-8979/83/020561-09$02.40

temperature compensation and/or substrate passivation, with the piezoelectric ZnO layer permitting transduction between electrical and acoustic energies. It is significant to note that recent results have shown that AlN could serve as an alternative to ZnO as a piezoelectric layer.[7]

In Sec. VII we discuss the variation in the first-order temperature coefficient of resonant frequency with SiO_2 thickness. When temperature compensation is desired, SiO_2 thickness is fixed with regard to wavelength with $h_2k = 0.47$; otherwise, a simple passivation layer is grown with a 0.1 μm nominal thickness.

The aluminum shorting plane of 0.1 μm thickness is vacuum deposited onto the SiO_2 layer. This conductive layer enhances electromechanical coupling while shielding mobile charge carriers in the silicon substrate from interacting with electric fields originating in the ZnO layer.[8] The wave-carrier interaction can cause a degree of Q-degrading acoustoelectric attenuation.

Onto the aluminum layer a ZnO layer is deposited by diode or rf magnetron sputtering with grains of the hexagonal structure having c axis oriented normal to the surface. Details of the sputtering procedure can be found in the literature.[9-11] The ZnO film thickness h_1 is typically 0.7–1.9 μm for devices operating near 100 MHz, and is determined by electromechanical coupling considerations. Figure 2 indicates the variation in electromechanical coupling $\Delta v/v$ with normalized ZnO thickness for both temperature compensating, and simple passivating thicknesses of SiO_2. From this figure it is seen that the presence of the temperature compensating SiO_2 layer on (111)-cut Si permits one to achieve usable $\Delta v/v$ values at a decreased ZnO layer thickness. For example, a typical $\Delta v/v$ value of 0.003 is obtained with any of the following configurations: ($h_1k = 0.24$, $h_2k = 0.02$, 111-cut Si), ($h_1k = 0.12$, $h_2k = 0.02$, 100-cut Si), ($h_1k = 0.11$, $h_2k = 0.47$, 111-cut Si). Two advantages result from allowing thinner ZnO layers to be used. First, it is easier to grow thin films of good quality than thicker ones. In particular, surface roughness is found to increase with ZnO film thickness. Second, the propagation loss, believed to be dominated by the polycrystalline ZnO film, is diminished by using a thinner layer.

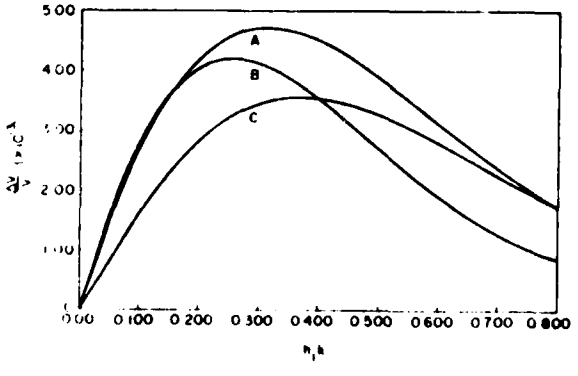

FIG. 2. Electromechanical coupling factor vs normalized ZnO thickness with (A) simple passivating SiO_2 thickness $h_2k = 0.02$ on (100)-cut Si; (B) temperature compensating SiO_2 thickness $h_2k = 0.47$ on (111)-cut Si; (C) simple passivating SiO_2 thickness $h_2k = 0.02$ on (111)-cut Si.

The Q-value obtained for a resonator is proportional to the ratio of stored energy to power dissipated, and is ultimately limited by propagation loss in the medium.[12] Thus, higher Q-values are obtained with the temperature compensated configuration using a thinner ZnO layer. For this configuration, measured Q-values in excess of 12 000 indicate an upper bound of 0.64 dB/cm for propagation loss at 123 MHz. Q-values are obtained by taking the reciprocal of the measured (3 dB) fractional bandwidth at resonance. In estimating loss mechanisms occurring in the resonant cavity, it is preferable to use devices whose transducers are weakly coupled to the resonant cavity, since electrical loading diminishes the apparent Q value. For cases where the coupling between input/output transmission lines and the resonant cavity was optimized for minimum insertion loss, the unloaded Q was determined by introducing shunt capacitance at the IDT terminals to decouple the cavity. In all cases measurements of cavity frequency response for the purpose of Q calculation were performed using a vector voltmeter together with a synthesized signal generator.

While obtaining low propagation loss is critical, the requirements on electromechancial coupling provided by the film are not. For off-resonant frequencies the transducer impedance level, proportional to $\Delta v/v$, is desired to be low in order that the impedance mismatch at device ports will result in a large rejection of out-of-band signals. Hence, maximum $\Delta v/v$, crucial for delay-line responses, is not required for resonator transducers. At resonance, it should be added, the impedance level of each transducer is increased drastically due to the location of the transducers in the resonant cavity, i.e., with IDT finger centers positioned at maxima of the standing wave potential. It is preferable to use a single masking step to define transducers and reflector arrays due to this stringent requirement on the positioning of transducer fingers with respect to the reflector arrays.

The planar features located on top of the ZnO, forming IDT's and distributed reflectors, are defined by standard photolithography. Several distributed reflector schemes have been tested, following the earlier development of single-crystal SAW resonators. Figure 3 illustrates portions of reflectors formed either from isolated metallic strips, shorted metallic strips, or grooves modulating the ZnO layer thickness. Again normalizing to acoustic wavenumber, the height of the wave-perturbing features in each case is denoted by hk, with $h < h_1$ in the case of grooves.

When metallic reflector gratings are used, transducers and reflectors are defined simultaneously from aluminum (by alkaline etching) or chrome-gold (by liftoff). The range of metal film thicknesses employed is 0.05–0.2 μm. When etched grooves are employed, aluminum transducers and reflector masking strips are defined simultaneously. Protecting the transducer region with photoresist, grooves are etched between masking strips. Chemical etching of the ZnO has been fairly successful, but is found to be surpassed in uniformity and repeatability by ion beam etching. A low energy argon beam is used, with an accelerating potential of 300 V, to minimize crystalline damage to the remaining ZnO. The ZnO etch rate is approximately 9% greater than that of aluminum when the ion beam is incident at 10° from

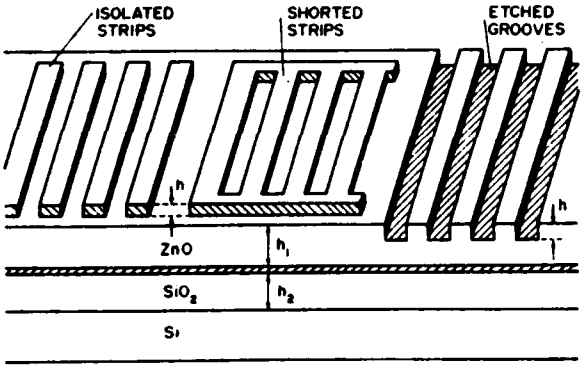

FIG. 3. Portions of distributed reflector arrays formed either from electrically isolated metallic strips, shorted metallic strips, or grooves modulating ZnO layer thickness. In each case, reflector array periodicity is half the acoustic wavelength.

normal. Proper choice of aluminum thickness permits simultaneous removal of masking strips with ZnO groove defintion.

The extent to which a Rayleigh wave is reflected by a small perturbing feature, such as a metal strip on, or groove in, the top layer, is dependent on the acoustic fields in that layer, and hence on the solution for the layered configuration. We have examined the reflection characterisitcs of an array of metal strips and grooves in several layer configurations. The selected configurations by no means exhaust the combinations of h_1k, h_2k, shorting plane, and substrate orientation which determine the acoustic and electrical properties obtainable in $ZnO/SiO_2/Si$ layered medium, but represent several found to be useful for resonator applications.

III. METAL REFLECTOR ARRAYS

There are several mechanisms whereby metal strips can give rise to a Rayleigh wave reflection[13], these are as follows:

(1) $\Delta v/v$ shorting: Conductive strips eliminate the tangential surface electric field, weakening piezoelectric stiffening. In the layered medium the result is a lowering of the Rayleigh velocity, and a decreased acoustic wave impedance;

(2) $\Delta v/v$ regeneration: For electrically isolated strips, the induced potential, which alternates between strips placed at half-wavelength intervals, regenerates a backward wave;

(3) Mass loading: When strips having a high mass density are used, each strip loads the wave, decreasing both the velocity and acoustic wave impedance;

(4) Topological discontinuity: As in the case of ridges or grooves etched in the surface, the field mismatch across a topological discontinuity caused by a metal strip may result in Rayleigh reflection.

The first two reflection mechanisms are dependent on electromechanical coupling strengh; thus the contribution from each can be controlled through ZnO thickness, h_1. The contribution from the last two mechanisms is determined primarily by metal thickness, h.

It is found that when aluminum reflector gratings are used, we must rely on $\Delta v/v$ reflection mechanisms. Since the maximum $\Delta v/v$ available from the $ZnO/SiO_2/Si$ configuration for the range of ZnO thicknesses usually available is 0.0045, we are thus limited to Rayleigh reflectivities of 0.5%. That the $\Delta v/v$ contributions actually outweigh mass loading or topological effects when using aluminum is evidenced by the measured phase reversal of reflection between isolated and shorted strips.

In the case of gold strips, however, the high mass density gives rise to a mass-loading contribution which is found to increase the net reflectivity of Rayleigh waves. Figure 4 shows the measured variation in reflectivity per quarter wave strip versus gold thickness h for a shorted chrome-gold grating on a particular layer configuration. (The thin chrome layer is present merely to insure adhesion of the gold.) The reflectivity per strip ρ referenced at the leading edge of a strip, is deduced from the measured data of Fig. 4 as

$$\rho = -1.4\frac{\Delta v}{v} - 0.34(hk). \tag{1}$$

It appears that the $\Delta v/v$ shorting and the mass-loading contributions are acting in phase. As the contribution from $\Delta v/v$ regeneration is 180° out of phase with these mechanisms, the most efficient metal grating Rayleigh reflectors are expected from shorted gold strips. Furthermore, with regard to these reflector arrays employing high mass density conductive strips, we note the following additional consideration. Since resistive losses are proportional to $\Delta v/v$, then for a constant gold thickness, reflector efficiency is expected to increase as $\Delta v/v$ is reduced. For this reason, a ZnO thickness is chosen which yields less than maximum $\Delta v/v$. As mentioned above, the use of a thinner ZnO layer also presents opportunities for higher Q values through a reduction in propagation loss in the ZnO.

Reflection magnitude of a particular surface perturbation scheme is determined experimentally by measuring the stop band depth of a signal transmitted through an array of 400 strips; the reflection phase is deduced from the standing wave pattern implied by the IDT positioning required for optimum coupling into a two-port resonator. Transducer location is generally specified by the distance of IDT finger centers from the reflector array edge. This has been experi-

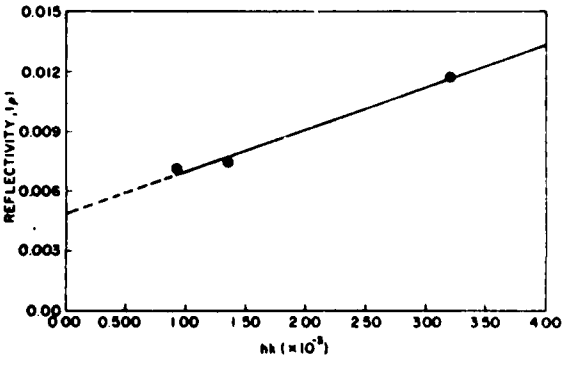

FIG. 4. Rayliegh-wave reflectivity per quarter-wave metallic strip vs normalized strip thickness for a reflector array formed from shorted Cr/Au strips on the layered configuration: $h_1k = 0.29$, $h_2k = 0.02$, (111)-cut Si.

mentally determined to be $[(n/2) + (1/4)]\lambda$ in the case of isolated or shorted Cr/Au strips or shorted aluminum strips, and $[(n/2)]\lambda$ in the case of isolated aluminum strips.

Figure 5 shows the two-port transmission characteristics of a resonator employing 400 shorted Cr/Au strips per array.

IV. GROOVE REFLECTOR ARRAYS

To eliminate losses associated with the conductivity of metal grating reflectors, it has been found advantageous to use etched groove reflector arrays. Modulating the ZnO layer thickness with etched grooves as indicated in Fig. 3, has resulted in effective distributed Rayleigh-wave reflectors. The wave reflection, occuring at the topological discontinuity associated with each change in ZnO thickness, is due to the mismatch between incident and transmitted acoustic fields. The reflectivity per groove ρ is found to increase linearly with groove depth as indicated in Fig. 6; that is, $\rho = \alpha hk$, in which α, the coefficient of reflectivity, varies with the layer configuration chosen. Comparing the cases graphed in Fig. 6, one concludes that the thick SiO_2 layer concentrates wave energy at the ZnO surface since a given groove depth provides some 3.5 times the reflectivity as the same groove without SiO_2.

An important characteristic associated with waveguiding structures is the associated velocity dispersion. In the layered acoustic medium under consideration, the presence of both the ZnO and SiO_2 layers decreases the wave velocity from that of the bare substrate in proportion to their normalized thicknesses h_1k, h_2k. Figure 7 illustrates the theoretical variation of velocity with normalized ZnO thickness for the temperature compensating and passivating thicknesses of SiO_2.

Since etching a groove in the ZnO layer acts to decrease the substrate loading in the etched region, the resultant wave velocity will be higher. This is neglecting, for the moment, the contribution made by energy storage at groove edges. Recourse to the velocity dispersion characteristics shown in Fig. 7 thus indicates a nearly linear increase in velocity with groove depth. This is in marked contrast to the nondispersive nature of single crystals, in which energy storage at surface discontinuities predominates to produce a decrease in velocity proportional to $(hk)^2$.[14]

In order to examine the variation in grating velocity perturbation with groove depth, test devices were designed to permit a phase comparison between signals transmitted through an unperturbed propagation track and one containing 200 grooves.[15] Figure 8 illustrates the observed first-order increase in grating velocity with groove depth for $hk < 0.80$. While no second order roll off from energy storage is evident in the cited experiment, it might become evident at larger relative groove depths. With linear velocity dispersion, and neglecting energy storage, the array velocity at the Bragg frequency is expected to depend on groove depth as (see Appendix A)

$$v_a = v_0(1 + rDhk), \tag{2}$$

where v_0 is the unperturbed Rayleigh velocity; r is the ratio of groove width to reflector periodicity; h is the groove depth; k

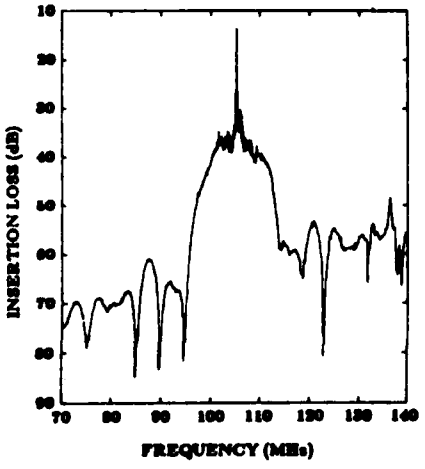

FIG. 5. Insertion loss measured between acoustic ports vs frequency for a resonator employing 400 shorted Cr/Au strips per reflector array. At resonance, the transmission is enhanced some 25 dB over the delay-line response.

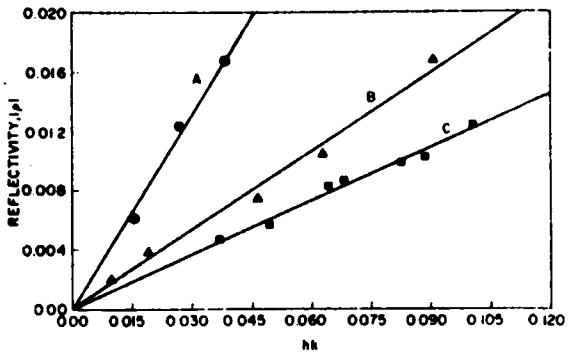

FIG. 6. Rayleigh-wave reflectivity per groove vs normalized groove depth for grooves modulating the ZnO layer of the following configurations: (A) $h_1k = 0.11$, $h_2k = 0.47$, (111)-cut Si; (B) $h_1k = 0.29$, $h_2k = 0.02$ (100)-cut Si; (C) $h_1k = 0.25$, $h_2k = 0.02$, (111)-cut Si.

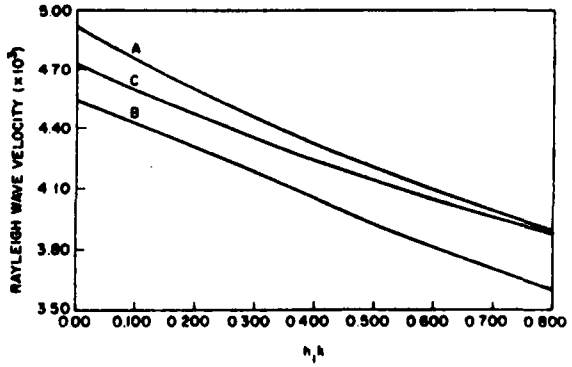

FIG. 7. Rayleigh-wave velocity vs normalized ZnO thickness for the SiO_2/substrate combinations examined in Fig. 2.

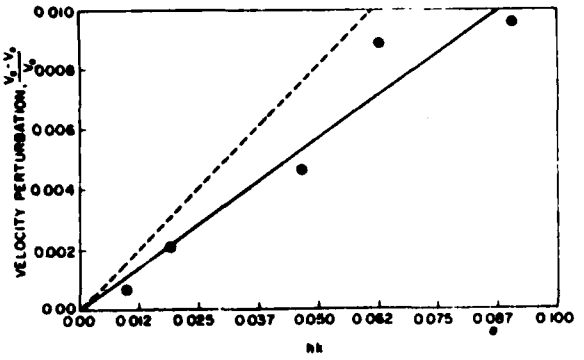

FIG. 8. Perturbation in groove reflector array phase velocity vs normalized groove depth in the ZnO layer. The dashed line is the perturbation calculated from dispersion considerations.

is the wave number; D is the fractional rate of decrease in Rayleigh-wave velocity with normalized ZnO thickness (the "dispersion"), defined by

$$D(h_1k,h_2k) = -\frac{1}{v_0}\frac{\partial v_0(h_1k,h_2k)}{\partial(h_1k)}. \tag{3}$$

Thus, calculating the velocity in the grating region as an appropriate average of the perturbed and unperturbed half-periods [Eq.(3)] yields the dashed line in Fig. 8.

Due to the dispersive nature of the medium, resonant frequency is sensitive to film thickness. Also, film thickness uniformity is important. Nonuniformity which results in a velocity gradient along a reflector array tends to produce a "chirp reflector," degrading reflection magnitude and increasing reflection bandwidth. The latter effect contributes to the emergence of spurious longitudinal modes. To obtain maximum uniformity along reflctors, ZnO sputtering is performed so that constant thickness contours tend to be parallel to the propagation direction.

V. DESIGN CONSIDERATIONS FOR A DISPERSIVE PROPAGATION MEDIUM

The velocity perturbation with groove depth must be considered in the design of SAW resonators for a dispersive medium. In order to realize a high-Q, single mode resonator, it is imperative that the resonant frequency coincide with the reflector center frequency.[16] To accomplish this, the phase shift between reflector array edges must be a multiple of π at the reflector center frequency. The difference in velocity perturbation caused by metal strips and grooves modifies the wavelength between the transducer region and the reflector array. Consequently, the specification of array separation and the location of transducer fingers in the resonant cavity is dependent upon the manner in which these features perturb the velocity of the medium, and hence upon the layered configuration employed.

For resonators built on single crystals and those using metal reflector gratings in the layered medium, the transducer and reflector elements each decrease the wave velocity only slightly so that resonance coincidence with reflector center is easily reconciled. In these cases, the velocity may usually be considered unchanged between regions. With groove resonators in the layered medium, however, the first-order increase in reflector array velocity, due to the presence of grooves, combined with a $\Delta v/v$ velocity reduction in the transducer region, produces a sizeable velocity differential between regions. Unless a corresponding variation is made in the reflector and interarray periodicities, the phase shift between arrays will not result in resonance at the reflector center frequency. Frequently the result of the misalignment is the introduction of spurious longitudinal modes. The cited velocity differential gives rise to the following relationship between the interarray wavelength λ_i and the reflector array wavelength λ_a:

$$\frac{\lambda_i}{\lambda_a} = \frac{1 - r_1 f\frac{\Delta v}{v}}{1 + r_2 Dhk}, \tag{4}$$

where f is the fraction of the array separation region occupied by transducers; r_1 is the fraction of the transducer period occupied by metallic fingers, while r_2 is the fraction of each array period occupied by grooves. (Typically $r_1 = r_2 = 0.5$.)

Given Eq. (4), one then proceeds as follows to generate a resonator pattern for use on the dispersive medium:

(a) Choose $\lambda_a/4$ to be a multiple of the pattern generator step size to enable equal groove/ridge spacing, as well as avoiding aliasing errors in the reflector array.

(b) For the layer configuration at hand, determine $\Delta v/v$ and groove depth h for the desired reflectivity. Calculating λ_i from Eq. (4), choose the array separation to be both a multiple of $\lambda_i/2$ and close to a multiple of the generator step size. The result will be the coincidence of resonance with the reflector center frequency.

(c) Generate reflectors with periodicity $\lambda_a/2$ and groove width $\lambda_a/4$. In the transducer region, finger centers are positioned $(n/2)\lambda_i$ from the reflector array edge. The transducer will have periodicity λ_i but is subject to any discretization error.

As has been mentioned above, the major poriton of the velocity differential between reflector and transducer regions is due to the velocity perturbation caused by grooves in the ZnO. The desired groove depth h_0 is dictated by the required level of reflectivity ρ_0 according to $\rho_0 = \alpha h_0 k$. Thus, for a given array reflectivity there results a fractional reflector velocity change given by

$$\frac{v_a - v_0}{v_0} = r_2\rho_0\left(\frac{D}{\alpha}\right). \tag{5}$$

We note that the influence of the layered medium is contained in the ratio of dispersion to the reflectivity gradient D/α. Although this velocity change has been accounted for in the design of the resonator pattern, a reproducibility problem arises when the groove depth realized deviates from the design value h_0. Any deviation in groove depth from h_0 results in a detuning of the reflector center frequency from resonance. The magnitude of this detuning is proportional to the fractional groove depth error and also to D/α. Consequently, those layered media yielding a minimum D/α value are the ones on which groove resonators are most easily im-

TABLE I. Properties of several ZnO/SiO_2/Si layer configurations.

Configuration			v_0(m/s)	$\frac{\Delta v}{v}$	D	α	$\frac{D}{\alpha}$
h_1k	h_2k	Si cut					
0.11	0.47	(111)	4410	0.0030	0.27	0.48	0.56
0.25	0.02	(111)	4390	0.0032	0.28	0.12	2.3
0.29	0.02	(100)	4460	0.0047	0.29	0.17	1.7

plemented. Table I lists the features of several possible configurations, including the figure of merit D/α. The values of α are obtained from measurements of reflectivity versus groove depth (Fig. 6).

From Table I we once again note the desirability of the thick SiO_2 sample, providing high reflectivity with dispersion essentially identical to the thin SiO_2 case. It is also significant to observe that the nearly linear dispersion characteristic associated with thin ZnO films allows a wide range of post-fabrication trimming (using ion beam etching) of resonant frequency without displaced resonance from the reflector center frequency.

VI. TRANSVERSE MODES AND IDT APODIZATION

Advantage may be taken of the velocity dispersion with ZnO layer thickness by constructing reflective arrays with waveguiding properties. In etching grooves in ZnO layer, the ZnO outside the beamwidth is simultaneously etched to the level of the groove depth as shown in Fig. 9. The uniformly etched region at the boundary of the reflector array thus has a higher Rayleigh velocity v' than does the array itself, offering greater lateral confinement of the acoustic beam.[17] One expects decreased diffraction loss as a result.

Transverse modes arise due to the finite width of the device. Each mode represents an eigenfunction satisfying the condition that the wave amplitude must go to zero outside the beamwidth of the device. Transverse modes can be thought of as arising from the propagation of a straight-crested wave at some small angle ϑ to the longitudinal axis. Since the angle increases for each higher order mode, corresponding parallel resonances are observed at successively higher frequencies.[18] The overall result is that a large number of transverse mode peaks are experimentally observed due to the waveguiding nature of the reflector array. These subsidiary peaks are evident as distortions on the high frequency side of the fundamental resonance response in the upper trace of Fig. 10. By analogy with the dielectric waveguide in electromagnetics, there are a limited number of confined modes. Those having a wavevector more oblique than some critical angle are leaky. The number of confined modes is proportional to the velocity differential across the reflector boundary ($v_a - v'$), which for a given array reflectivity is proportional to D/α.

An explicit and fairly accurate determination of the transverse mode resonances can be made by modeling the resonator as a two-dimensional box whose boundaries are the beamwidth and effective cavity length of the device.

The longitudinal axis lies along a pure mode propagation direction of the silicon substrate. Deviation from this axis results in an approximately parabolic velocity variation[19]:

$$v(\vartheta) = v_{0i}(1 - \eta\vartheta^2), \tag{6}$$

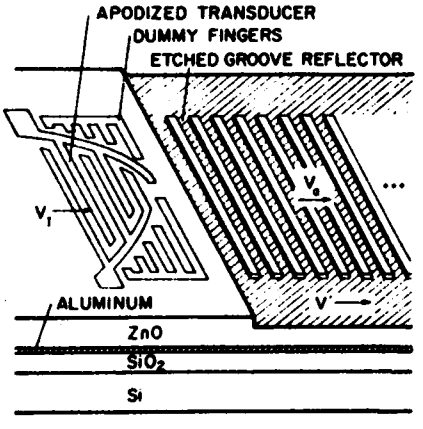

FIG. 9. Increased velocity v' alongside the etched groove (ridge) reflector array leads to a highly overmoded resonator. A transducer employing fingers of varying active length is used to couple preferentially to the fundamental transverse mode. The presence of the ground plane necessitates a modification of the apodization scheme used in single crystal substrates.

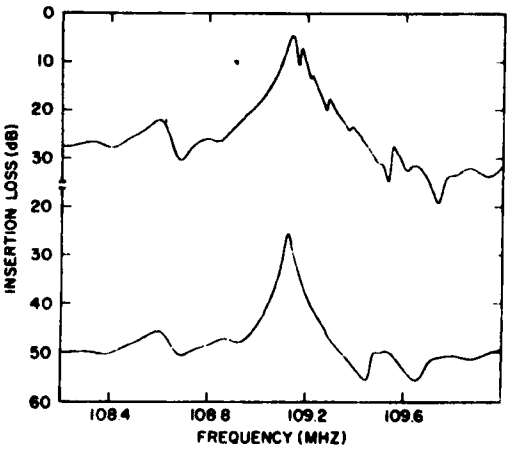

FIG. 10. Two-port resonator transmission responses with uniform transducer (top), and using the proposed finger-length apodization scheme (bottom).

where ϑ is a small angular deviation from a pure mode direction and η related to the propagation anisotropy. The transverse mode spectrum is heavily dependent on substrate anisotropy and is given by (Appendix B)

$$\Delta f_n = f_n - f_1 = \frac{f_1 \gamma^2 (n^2 - 1)}{8 w_p^2}, \quad n = 2,3,4,..., \tag{7}$$

where w_p is the beamwidth of the device in wavelengths and $\gamma = (1 - 2\eta)^{1/2}$ is the anisotropy factor. The value of γ is 0.53 for the (111) cut, $\langle 2\bar{1}\bar{1} \rangle$ propagation direction, and 1.1 for the (100) cut, $\langle 010 \rangle$ propagation direction in silicon. The anisotropy is modified slightly by the presence of the SiO_2 and ZnO layers, the layers tending to make the medium more isotropic. With a uniform transducer, resonances are observed on the high frequency side of the fundamental at frequencies f_n for $n = 3,5,7,9,...$ corresponding to the higher order symmetric modes. These modes are clearly evident in the upper trace of Fig. 10.

The distortion of ideal amplitude and phase response characteristics caused by the presence of the transverse mode resonances is undesirable. In order to couple preferentially to the fundamental transverse mode and eliminate excition of higher-order resonances, it is necessary to apodize the transducers, weighting the coupling across the beam path according to the fundamental mode shape.[20] Tailoring finger overlap is an effective means of apodization in transducers built on single-crystalline substrates, where that portion of each finger which is adjacent to one of opposite polarity is effective in coupling to an acoustic wave. The conventional method of weighting, however, is ineffective for transducers on a layered medium employing a ground plane. In the layered medium the piezoelectric thickness is normally much less than the transducer periodicity, with the conductive plane providing capacitive coupling between entire combs of the transducer. (In fact, Melloch *et al.* have shown that only one comb is necessary for effective transduction in the presence of a ground plane.[21])

In the layered configuration finger lengths must thus be tailored to provide weighting, or alternatively the ground plane must be suitably shaped to weight portions of fingers lying immediately above. Approximating the fundamental transverse mode shape by a cosine function, Fig. 9 shows an apodization scheme designed to couple preferentially to the fundamental mode in the layered medium. Dummy fingers are included which are not electrically connected to either terminal, but serve to equalized the velocity perturbation across the beam path. The effect of the dummy fingers on device Q has been inconclusive to date. A comparison of two-port resonator responses between the apodized transducer and one employing uniform finger lengths is shown in Fig. 10. Both resonators were fabricated on the same wafer. Due to the increase in bus-bar capacitance, the apodized transducer exhibits greater insertion loss. Apodized transducer coupling may be increased by minimizing bus-bar capacitance, optimization of acoustic beamwidth, or by inductive tuning.

VII. TEMPERATURE COMPENSATING THE LAYERED STRUCTURE

For the majority of applications requiring an extremely narrow bandpass filter, the stability of the center frequency must be on the order of the bandwidth. It is imperative, therefore, that SAW resonators contemplated for such use have a resonant frequency stable over time and temperature variation. With regard to aging characteristics, the only observation to date has been a significant increase in resonant frequency for devices exposed to the atmosphere. Since this effect is reversed by high temperatures or low pressures, it is attributed to moisture absorption by the ZnO layer. Aging studies of hermetically sealed devices remain to be performed.

The temperature stability of a SAW substrate material is usually specific in terms of a first-order temperature coefficient of phase delay, defined as

$$TC_{pd} = \frac{1}{\tau}\frac{d\tau}{dT} = \frac{1}{L}\frac{dL}{dT} - \frac{1}{v}\frac{dv}{dT}. \tag{8}$$

Note that this quantity is dependent on both changes in dimension of the medium in the direction of propagation, L, as well as changes in phase velocity, v, with temperature.[22] A SAW resonator displays a first order temperature coefficient of resonant frequency TC_f, which is the negative of TC_{pd}. Resonators built on $LiNbO_3$, for example, drift at a rate of 80 ppm/°C near room temperature. The single crystalline substrate of current practical value yielding the lowest TC_{pd} value is the ST cut of quartz.

Rather than be constrained to using a temperature stable substrate, it is possible to obtain a stable structure by adding a temperature compensating layer. For example, a layer having a TC_{pd} of the opposite sign can be added to the substrate to form a temperature stable composite. The temperature compensation, dependent on film thickness relative to SAW wavelength, will be effective only within a narrow frequency range. This behavior is not objectionable for resonator use, but may be undesirable for broad-band devices. Silicon dioxide, unusual in having a negative TC_{pd}, has often been used as a compensating layer on piezoelectric substrates such as the YZ cuts of $LiNbO_3$, and $LiTaO_3$.[23] The SiO_2 layer is typically sputtered onto these substrates.

Silicon dioxide is particularly attractive as a compensating layer on the silicon substrate because high quality, precisely controlled SiO_2 films can be obtained by thermal growth. Groove resonators were constructed using various thicknesses of thermal SiO_2 in an attempt to find a temperature compensated $ZnO/SiO_2/Si$ configuration. Figure 11 shows the variation found in the first-order temperature coefficient of frequency (TC_f) at 23° C for a structure consisting of a $ZnO/SiO_2/Si$ resonator bonded with silver epoxy to a steel header; the normalized SiO_2 thickness is h_2k. Without SiO_2, $TC_f = -25$ ppm/° C; TC_f increases with SiO_2 thickness reaching zero when $h_2k = 0.47$. While predictions have been made[24] concerning the influence of ZnO thickness and grooves in the ZnO layer on TC_f we have thus far found such factors to have negligible effect. Thus, coupling considerations alone determine ZnO thickness in the temperature

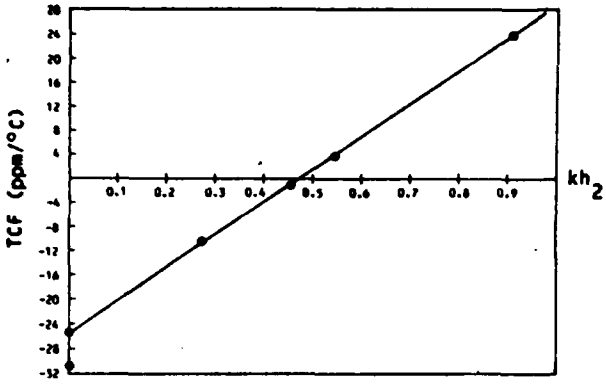

FIG. 11. First-order temperature coefficient of resonant frequency vs normalized SiO_2 thickness. For etched-groove resonators on (111)-cut Si at 23 °C.

compensated configuration. It is expected that the nature of the mounting configuration will affect the temperature characteristics.

A ZnO/SiO_2/Si resonator, mounted on a steel header, has been constructed with $h_2k = 0.46$. The resulting temperature stability is shown in Fig. 12 and is compared to uncompensated and overcompensated characteristics. In addition, experimental results for ST quartz are included for comparison.[25]

A feature of the layered configuration is an ability to vary the turnover temperature of the resonator by changing the h_2k value. The second order temperature coefficient remains nearly unchanged, having a value of -0.052 ppm/deg. C)[2].

It has been apparent at several points in this paper that the advantages of using a thick SiO_2 layer have been found to go beyond that of achieving temperature stabilization. Once again referring to Fig. 2, we see that the temperature compensating SiO_2 thickness causes a more rapid increase in electromechanical coupling with ZnO thickness. Consequently a thinner ZnO layer is normally used; typically

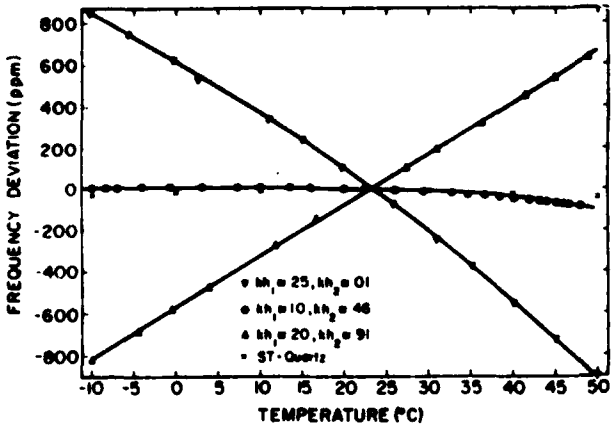

FIG. 12. Deviation in resonant frequency from room temperature (23 °C) value vs temperature. Undercompensation, compensation, and overcompensation are exhibited for various values of normalized SiO_2 thickness and are compared with reported ST-quartz behavior.

$h_1k = 0.11$. In addition, the low ratio of dispersion to reflectivity gradient D/α obtained with the temperature compensating SiO_2 layer, results in less reflector velocity perturbation for a given reflectivity.

VIII. CONCLUSION

We have detailed the manner in which temperature compensated SAW resonators can be implemented on a ZnO/SiO_2/Si layered medium. As in the case of single-crystal devices, metal reflector gratings can be used; here the layered medium offers variability in the contribution from each reflection mechanism through control of the metal/ZnO thicknesses. The most efficient reflectors are realized using etched groove arrays, but these present additional problems due to the velocity dispersion associated with the layered medium. However, grooved array design difficulties can be minimized by choosing a layer configuration (h_1k, h_2k, substrate) displaying a minimum value of D/α.

It has been shown that prominent transverse mode resonances arise with normal beamwidths, but the undesireable effects can be suppressed with a novel transducr design. Finally, the ZnO-on-Si SAW resonator, potentially useful as a fully integrated semiconductor component, is also promising as a tool for further reasearch on layered media.

ACKNOWLEDGMENTS

The authors would like to thank G. MaGee of the Naval Avionics Center for assistance in making photomasks, as well as Dr. R. Razouk and L. Lie of Fairchild Corporation for preparing thick silicon dioxide samples. The authors appreciate many useful discussions with Professor S. Datta. This research was sponsored jointly by AFOSR grant AF810214 and NSF-MRL grant 8020249.

APPENDIX A: CALCULATION OF GROOVE REFLECTOR ARRAY VELOCITY

The center frequency of the reflector array is that which results in a π phase shift per reflector period. Due to the dispersive nature of the layered medium, the groove portion of each reflector period has a higher Rayleigh velocity than does the unetched portion; thus, the array consists of regions of alternating velocity values. By "array velocity," we mean to associate a single velocity with the array which would result in the same Bragg frequency, i.e., $v_a = 2f_c\Lambda$ where Λ is the array periodicity. Letting s be the groove width in each periodic section, the phase shift per period is given by

$$\varphi(f) = 2\pi f\left(\frac{s}{v_1} + \frac{\Lambda - s}{v_0}\right), \tag{A1}$$

where v_0, v_1 denote Rayleigh velocities in the unetched and etched portions of the reflector period, respectively. At the reflector center frequency f_c we have $\varphi(f_c) = \pi$ and $v_a = 2f_c\Lambda$, so that the array velocity is given by

$$v_a = \frac{\Lambda}{\frac{s}{v_1} + \frac{\Lambda - s}{v_0}}. \tag{A2}$$

From the nearly linear velocity characteristics of Fig. 7, we

can write the groove velocity in terms of the unperturbed velocity as

$$v_1 = v_0[(h_1 - h)k, h_2 k]$$
$$= v_0(h_1 k, h_2 k) - \left[\frac{\partial v_0(h_1 k, h_2 k)}{\partial(h_1 k)}\right] hk, \quad \text{(A3)}$$

in which h is the groove depth, h_1 the unetched ZnO thickness, and h_2 the SiO_2 thickness. Defining D as

$$D = -\frac{1}{v_0}\frac{\partial v_0(h_1 k, h_2 k)}{\partial(h_1 k)}, \quad \text{(A4)}$$

we have the groove velocity

$$v_1 = v_0(1 + Dhk). \quad \text{(A5)}$$

Substituting this expression into Eq. (A2), the array velocity may be written as

$$v_a = \frac{v_0(1 + Dhk)}{1 + (1 - r)Dhk}. \quad \text{(A6)}$$

For $Dhk \ll 1$, the array velocity is given by the simplified expression

$$v_a = v_0(1 + rDhk). \quad \text{(A7)}$$

APPENDIX B: CALCULATION OF TRANSVERSE MODE SPECTRUM

The SAW resonator is modeled as a two-dimensional cavity whose length is the effective cavity length L and whose width is the actual device width w. A resonance condition is satisfied whenever

$$k_x = \frac{m\pi}{L}, \quad k_y = \frac{n\pi}{w}, \quad m,n = 1,2,3,..., \quad \text{(B1)}$$

where k_x is the wavenumber along the length of the device, and k_y the wavenumber in the transverse direction. Due to the anisotropy of the crystalline substrate.

$$v(\vartheta) = v_0(1 - \eta\vartheta^2), \quad \text{(B2)}$$

so that the resultant k vector can be written as

$$\mathbf{k} = k_x\bar{x} + \gamma k_y\bar{y}, \quad \text{(B3)}$$

with $\gamma = (1 - 2\eta)^{1/2}$. Then the resonant frequencies are given by

$$\omega_{m,n}^2 = v^2k^2 = v^2\left[\left(\frac{m\pi}{L}\right)^2 + \gamma^2\left(\frac{n\pi}{w}\right)^2\right]. \quad \text{(B4)}$$

The narrow reflector bandwidth limits the cavity to a single longitudinal mode, $m = m_0$. The frequency interval between the fundamental transverse mode (m_0, 1) resonances and higher order transverse mode resonances (m_0, n) is given by

$$\omega_{m_0,n}^2 - \omega_{m_0,1}^2 = \left(\frac{\gamma\pi v}{w}\right)^2(n^2 - 1), \quad n = 2,3,4,..., \quad \text{(B5)}$$

or approximately,

$$2\omega_{m_0,1}(\omega_{m_0,n} - \omega_{m_0,1}) = \left(\frac{\gamma\pi v}{w}\right)^2(n^2 - 1), \quad n = 2,3,4,.... \quad \text{(B6)}$$

Thus, the transverse mode spectrum is given by

$$\Delta f_n = f_n - f_1 = \frac{f_1\gamma^2(n^2 - 1)}{8w_p^2}, \text{ with } w_p = \frac{w}{\lambda}. \quad \text{(B7)}$$

[1] R. L. Rosenberg, D. G. Ross, and P. R. Trischitta, in *1981 Ultrasonics Symposium Proceedings, Chicago* (IEEE, New York, 1981), p. 332.
[2] S. J. Martin, R. L. Gunshor, and R. F. Pierret, Appl. Phys. Lett. **37**, 700 (1980).
[3] S. J. Martin, R. L. Gunshor, and R. F. Pierret, in *1980 Ultrasonics Symposium Proceedings, Boston* (IEEE, New York, 1980), p. 113.
[4] E. A. Ash, IEEE Symposium of Microwave Theory and Techniques, Newport Beach, 1970 (unpublished).
[5] E. J. Staples, J. S. Schoenwald, R. C. Rosenfeld, and C. S. Hartmann, in *1974 Ultrasonics Symposium Proceedings, Milwaukee* (IEEE, New York, 1974), p. 245.
[6] G. S. Kino and R. S. Wagers, J. Appl. Phys. **44**, 1480 (1973).
[7] L. G. Pearce, R. L. Gunshor, and R. F. Pierret, Appl. Phys. Lett. **39**, 878 (1981).
[8] R. L. Gunshor, Solid State Electron. **18**, 1089 (1975).
[9] T. Shiosaki, in *1978 Ultrasonics Symposium Proceedings, Cherry Hill* (IEEE, New York, 1978), p. 100.
[10] B. T. Khuri-Yakub, G. S. Kino, and P. Galle, J. Appl. Phys. **46**, 3266 (1975).
[11] F. S. Hickernell, in *1980 Ultrasonics Symposium Proceedings, Boston* (IEEE, New York, 1980), p. 785.
[12] E. J. Staples and R. C. Symthe, in *1975 Ultrasonics Symposium Proceedings, Los Angeles* (IEEE, New York, 1975), p. 307.
[13] C. Dunrowicz, F. Sandy, and T. Parker, in *1976 Ultrasonics Symposium Proceedings, Annapolis* (IEEE, New York, 1976), p. 386.
[14] R. C. M. Li, J. A. Alusow, and R. C. Williamson, in *Proceedings, 29th Annual Symposium on Frequency Control, Philadelphia* (US Army Electronics Command, Fort Monmouth, New Jersey, 1975), p. 167.
[15] W. J. Tanski, IEEE Trans. Sonics Ultrason. **SU-26**, 815 (1979).
[16] W. J. Tanski and H. Van de Vaart, in *1977 Ultrasonics Symposium Proceedings, Phoenix* (IEEE, New York, 1977), p. 160.
[17] H. A. Haus, J. Appl. Phys. **48**, 4955 (1977).
[18] J. Schoenwald, in *Proceedings, 30th Annual Symposium on Frequency Control, Philadelphia* (US Army Electronics Comand, Fort Monmouth, New Jersey, 1976), p. 340.
[19] A. J. Slobodnik, Jr., Proc. IEEE **64**, 581 (1976).
[20] W. R. Shreve, in *Proceedings, 30th Annual Symposium on Frequency Control, Philadelphia* (US Army Electronics Command, Fort Monmouth, New Jersey, 1976), p. 328.
[21] M. R. Melloch, R. L. Gunshor, and R. F. Pierret, IEEE Trans. Sonics Ultrason. **SU-29**, 55 (1982).
[22] R. W. Weinert and T. J. Isaacs, in *Proceedings, 29th Annual Symposium on Frequency Control, Philadelphia* (US Army Electronics Command, Fort Monmouth, New Jersey, 1975), p. 139.
[23] T. E. Parker, M. B. Shulz, and H. Wichansky, in *Proceedings, 29th Annual Symposium on Frequency Control, Philadelphia* (US Army Electronics Command, Fort Monmouth, New Jersey, 1975), p. 143.
[24] G. Cambon, E. L. Alder, J. Attal, and W. Shahab, in *1979 Ultrasonics Symposium Proceedings, New Orleans* (IEEE, New York, 1979), p. 637.
[25] D. Hauden, M. Michel, G. Bardeche, and J. J. Gagnepain, Appl. Phys. Lett. **31**, 315 (1977).

APPENDIX D

SAW Resonators on Silicon

S. J. Martin, S. Datta, R. L. Gunshor, R. F. Pierret,
M. R. Melloch*, and E. J. Staples**

School of Electrical Engineering, Purdue University
West Lafayette, IN 47907

SAW resonators have been successfully demonstrated on the $ZnO/SiO_2/Si$ layered medium. Distributed reflector arrays, central to these devices, can be formed by modulating the ZnO layer thickness with grooves. The Rayleigh wave reflectivity and velocity perturbation caused by these grooves are examined along with the resulting resonator design considerations.

Layer configurations may be formed which support a higher order (Sezawa) propagating mode in addition to the lowest order (Rayleigh) mode. Perturbations on the surface of such media scatter wave energy between modes in such a way that distributed mode converting reflectors may be formed. Resonators have been constructed which utilize both propagating modes and offer potential advantages for improving out-of-band signal rejection.

A theoretical model based on the normal mode theory of Auld has been developed which allows Rayleigh wave reflectivity and mode conversion magnitudes to be calculated. Theoretical results compare favorably with experimental values, particularly for scattering from Sezawa to Rayleigh modes.

I. Introduction

This paper describes recent developments in surface acoustic wave (SAW) resonators fabricated on a $ZnO/SiO_2/Si$ layered medium. Adaptation of SAW resonator technology to silicon has paralleled the prior resonator development on piezoelectric single-crystalline materials such as quartz and lithium niobate [1-2]. Initially metal strip reflectors were used [3]; subsequently etched grooves were found to produce the most efficient distributed reflectors [4]. Use of etched grooves in the dispersive layered medium, however, gives rise to a first-order velocity perturbation. This velocity perturbation leads to unique resonator design considerations. Also in contrast to devices constructed on single crystals, resonators constructed on the layered medium may utilize a higher order propagating mode.

The motivation for using silicon as a substrate lies in the possibility of incorporating the SAW resonator in monolithic integrated circuits. Envisioned applications include frequency control of on-chip oscillators, digital PCM regenerators, pressure and acceleration sensors, etc.

II. Device Structure

The configuration for the two port SAW resonator on a $ZnO/SiO_2/Si$ layered medium is shown in Fig. 1. In fabricating the devices, both (100) and (111) cuts of silicon have been used as substrates, with wave propagation along the $<010>$ and $<2\bar{1}\bar{1}>$ directions, respectively. These pure mode directions result in a decoupling of the transverse mode from the sagittal mode. With the SiO_2 and ZnO layer thicknesses normally employed, only the lowest order sagittal or Rayleigh-like propagating mode may be excited by means of an interdigital transducer (IDT).

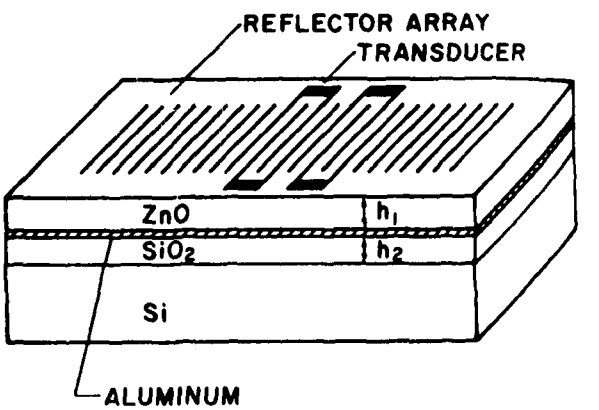

Fig. 1. SAW two-port resonator using piezoelectric ZnO layer on thermally oxidized Si substrate.

The RF sputtered piezoelectric ZnO layer permits transduction between electrical and acoustic energies on the non-piezoelectric Si/SiO_2 substrate. The ZnO thickness, whose normalized value is denoted by h_1k, is chosen to yield a moderate value of electromechanical coupling; typically $\Delta v/v = 0.003$ [5]. The thermally grown SiO_2 layer provides control of the temperature characteristics of resonant frequency. By proper choice of SiO_2 thick-

* Present address: Central Research Labs, Texas Instruments, Dallas, TX 75265.
** Present address: Microelectronics Research and Development Center, Rockwell International, Thousand Oaks, CA 91360.

ness, whose normalized value is denoted h_2k, temperature stability on the order of ST-quartz may be achieved. The aluminum ground plane between the SiO_2 and ZnO layers, having 0.1 μm nominal thickness, serves to enhance $\Delta v/v$ and also tends to decouple mobile charge carriers in the substrate from electric fields in the ZnO. The planar features on top of the ZnO include IDT's positioned inside a resonant cavity formed by two etched groove reflector arrays. The grooves in the top of the ZnO layer are formed by ion beam etching.

III. Reflector Array Characteristics

The periodic modulation of ZnO thickness by etched grooves causes reflection of an incident Rayleigh wave at the Bragg wavelength. The reflection magnitude of each groove depends on groove depth and also on the wave distribution in the surface-normal direction of the layered medium.

A series of measurements have been made to determine the magnitude of reflection of a Rayleigh wave due to a groove in the ZnO layer. By noting the stop-band depth for an acoustic signal transmitted through an array of grooves, the reflection magnitude per groove was determined [6]. As seen from the experimental points in Fig. 2, Rayleigh wave reflectivity increases linearly with normalized groove depth, denoted by hk. Reflection magnitude is also seen to depend substantially on the layer configuration (h_1k, h_2k, and substrate orientation) which determines the acoustic wave distribution.

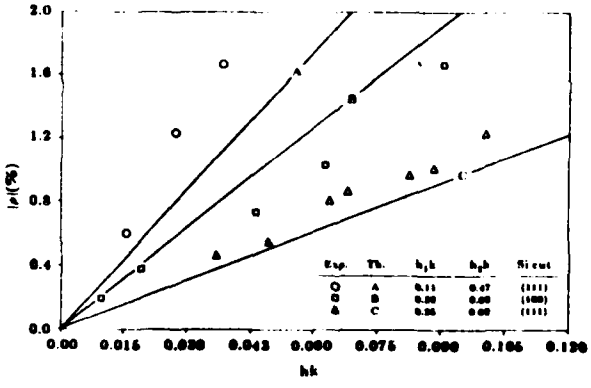

Fig. 2. Rayleigh-wave reflectivity per groove vs. normalized groove depth for grooves in the ZnO layer of several layer configurations.

The reflection of Rayleigh waves from grooves in single material substrates has been treated by Datta and Hunsinger [7] using the normal mode theory of Auld [8]. The same method was exended to the layered $ZnO/SiO_2/Si$ medium with the results indicated by solid lines in Fig. 2. The details of this calculation will be published shortly.

Due to the dispersive nature of the layered medium, modulation of the ZnO thickness by reflector array grooves causes an increase in phase velocity and consequently an increase in the Bragg frequency. By measuring the phase shift between acoustic signals transmitted through an unperturbed track and one containing 200 grooves, the velocity perturbation caused by etched grooves was measured. As indicated by the experimental points in Fig. 3, a linear increase in array velocity with groove depth is observed.

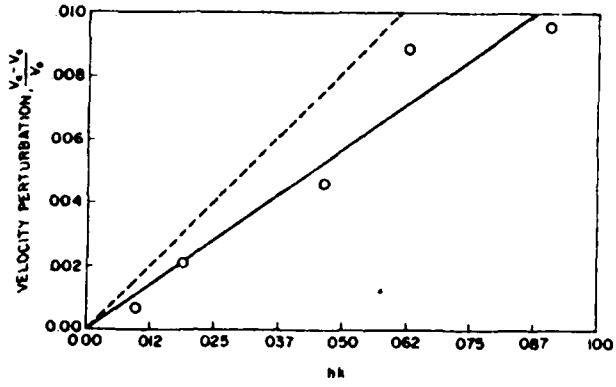

Fig. 3. Perturbation in groove reflector array phase velocity vs. normalized groove depth in the ZnO layer.

Assuming a linear velocity change over small ranges of ZnO thickness, and neglecting energy storage at groove edges, the array velocity, v_a, is expected to depend on groove depth as

$$v_a = v_o(1 + rDhk) \tag{1}$$

where v_o is the unperturbed Rayleigh velocity, r is the ratio of groove width to reflector periodicity, h is the groove depth, k is the Rayleigh wavenumber, and D is the fractional rate of decrease in Rayleigh wave velocity with normalized ZnO thickness (the "dispersion") defined by:

$$D(h_1k,h_2k) = -\frac{1}{v_o}\,\frac{\partial v_o(h_1k,h_2k)}{\partial(h_1k)}. \tag{2}$$

Calculating the velocity in the array in this manner yields the dashed line in Fig. 3.

IV. Design Considerations Due to Velocity Dispersion

The velocity perturbation caused by grooves must be considered when designing SAW resonators for a dispersive medium. In order to obtain a high-Q, single mode resonator, it is imperative that the resonant frequency coincide with the reflector center frequency. With groove resonators in the layered medium, the first-order increase in reflector array velocity (due to grooves), combined with a $\Delta v/v$ velocity reduction in the transducer region, produces a sizeable velocity differential between regions.

Unless a corresponding variation is made in the reflector and inter-array periodicities, the phase shift between arrays will not result in resonance at the reflector center frequency. The cited velocity differential gives rise to the following relationship between inter-array wavelength λ_i, and the reflector array wavelength λ_a:

$$\frac{\lambda_i}{\lambda_a} = \frac{1 - r_1 f \frac{\Delta v}{v}}{1 + r_2 Dhk} \qquad (3)$$

where f is the fraction of the array separation region occupied by transducers, r_1 is the fraction of the transducer period occupied by metallic fingers, while r_2 is the fraction of each reflector array period occupied by grooves. Determining D and $\Delta v/v$ for the layer configuration to be employed, one can adjust inter-array and reflector periodicities according to Eq. 3. When the reflector periodicity is a multiple of $\lambda_a/2$ and the reflector separation is a multiple of $\lambda_i/2$, then resonance will occur at the reflector center frequency. Resonators so designed exhibit a single resonance mode. Device Q-values are typically in the range of 3,000 to 12,000 for resonant frequencies near 100 MHz, decreasing as 1/f at higher frequencies.

V. Ageing Characteristics

Recently a month long pre-ageing study of $ZnO/SiO_2/Si$ resonators fabricated in our laboratory was conducted at Rockwell International [9]. Several devices were attached to dual in-line headers using gold wire bonds to strap down the substrate. This method of mounting eliminates age-inducing stresses which might arise if the substrates were bonded to headers. After bonding to the device, a 24 hour vacuum bakeout at 125° C was performed. Steel lids were then welded under vacuum onto the package bases to hermetically seal the devices.

Ageing tests of five devices were performed by monitoring the impedance at each transducer port. Two traces per plot are shown in Fig. 4 representing the change in resonant frequency for each resonator port. The devices were maintained at 85° C for the duration of the test. All of the devices exhibit a rapid increase in frequency of from 15 to 50 ppm over the first 24 hours. The cause of this initial jump in frequency is unknown. The subsequent gradual decline in resonant frequency for some devices is characteristic of a failure to achieve a hermetic seal in device packaging. Two of the devices, however, display promising ageing characteristics, drifting less than 10 ppm during the subsequent ageing period.

VI. Devices Utilizing Two Propagating Modes.

In a layered $ZnO/SiO_2/Si$ medium for which h_1k is sufficiently large, it is possible to propagate a second order sagittal mode in addition to the fundamental Rayleigh mode. Using a (100)-cut Si substrate, with wave propagation in the <010> direction, for example, this

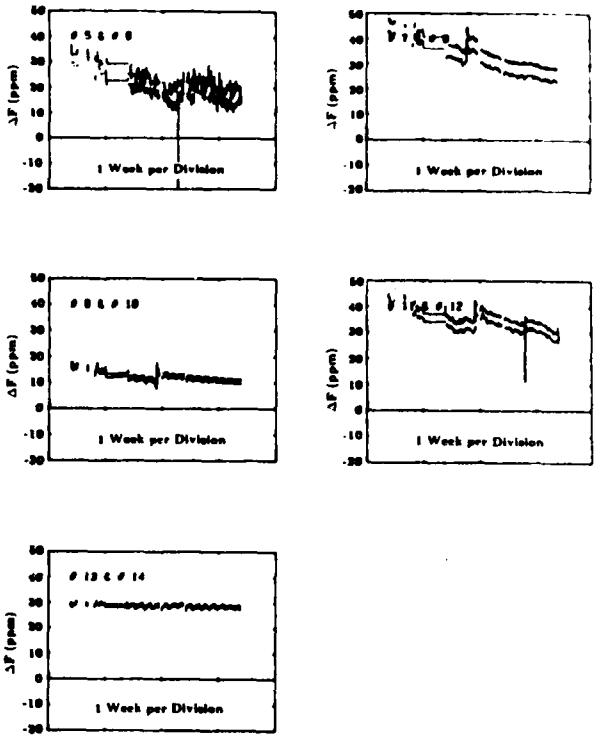

Fig. 4. Ageing characteristics of several hermetically packaged $ZnO/SiO_2/Si$ SAW resonators.

second order "Sezawa" mode will propagate when $h_1k > 0.8$ [10]. The Sezawa mode is characterized by a higher phase velocity and $\Delta v/v$ than is the Rayleigh mode.

Melloch et al [11] demonstrated that when a propagating mode of one type is incident on an array of grooves or metal strips having the proper periodicity, energy can be coherently scattered into the other propagating mode. One periodic section of a mode conversion reflector is illustrated in Fig. 5. The fundamental coherent reflection between Rayleigh and Sezawa modes occurs when

$$k_R + k_S = \frac{2\pi}{d} \qquad (4)$$

where k_R and k_S are the Rayleigh and Sezawa wavenumbers (positive irrespective of direction), and d is the array periodicity.

Measurements have been made to determine the scattering magnitude between an incident Sezawa wave and backward Rayleigh wave due to a groove in the ZnO layer. Using the procedure described previously (for determining Rayleigh reflectivities), the Sezawa-to-Rayleigh scattering magnitude, denoted $|\rho_{SR}|$, can be deduced from the stop band depth accompanying Sezawa wave transmission through a mode converting array. As each mode has a unique wave distribution, the meaning of an amplitude reflection coefficient is unclear. Conse-

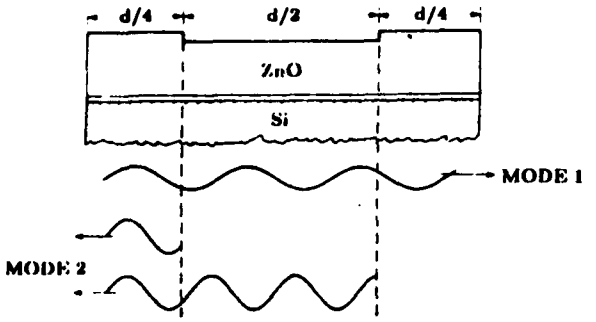

Fig. 5. One periodic section of a mode-converting reflector array.

quently, we define:

$$\left|\rho_{SR}\right| = \sqrt{\frac{P_{R-}}{P_{S+}}} \qquad (5)$$

where P_{S+} is the time-averaged incident Sezawa wave power and P_{R-} is the time- averaged reflected Rayleigh wave power. The normal mode theory has been extended to calculate mode conversion reflectivity. The result, indicated by a solid line in Fig. 6, is seen to agree very well with experimental measurements.

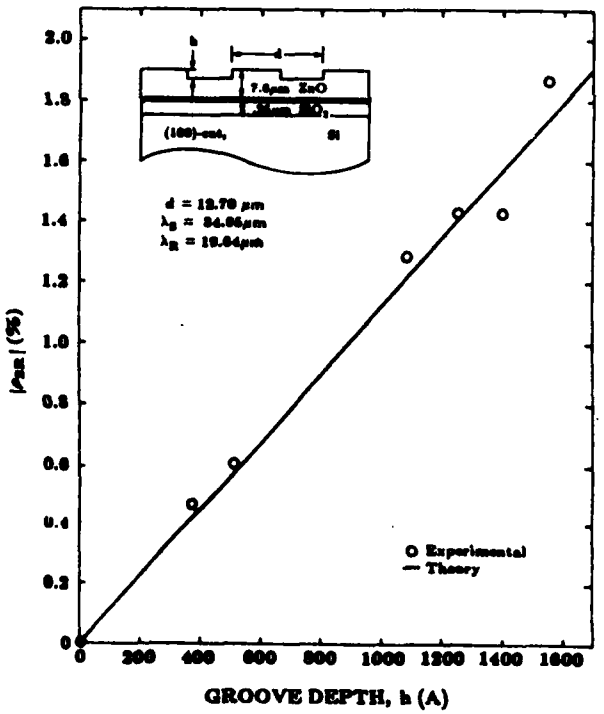

Fig. 6. Magnitude of Sezawa-to-Rayleigh mode scattering vs. groove depth in the ZnO layer.

In a layered acoustic medium which supports two propagating modes, reflection between modes of the same type remains possible when the usual Bragg condition is satisfied. However, the ability to convert between modes upon reflection affords potential advantages in resonator performance, particularly with regard to improving out-of-band signal rejection.

A resonant cavity may be formed between two mode-converting reflector arrays. A Rayleigh wave traversing the resonant cavity in one direction will be reflected as a Sezawa wave at the same frequency, provided Eq. 4 is satisfied. After traversing the cavity in the opposite direction as a Sezawa wave, it will be re-reflected as a Rayleigh wave. A resonance condition is satisfied whenever the round trip phase shift is a multiple of 2π.

In one version of the mode conversion resonator, one transducer having periodicity λ_R is placed in the resonant cavity to couple optimally to the resonant standing Rayleigh wave, while a second transducer having periodicity λ_S is placed to couple optimally to the standing Sezawa wave. Outside of the mode conversion bandwidth of the reflector array the difference in transducer periodicities reduces the acoustic transmission level between ports, thereby increasing the rejection level of the device.

The frequency response of a mode conversion resonator is shown in Fig. 7. The device Q is approximately 3,000, indicating that mode conversion reflectors operate efficiently without excessive losses to spurious modes. In fact, the device Q is thought to be limited primarily by propagation loss occurring in the 6.5 μm ZnO film. Out-of-band signal rejection could be enhanced, we feel, by apodizing transducers so that each couples only to its designated mode.

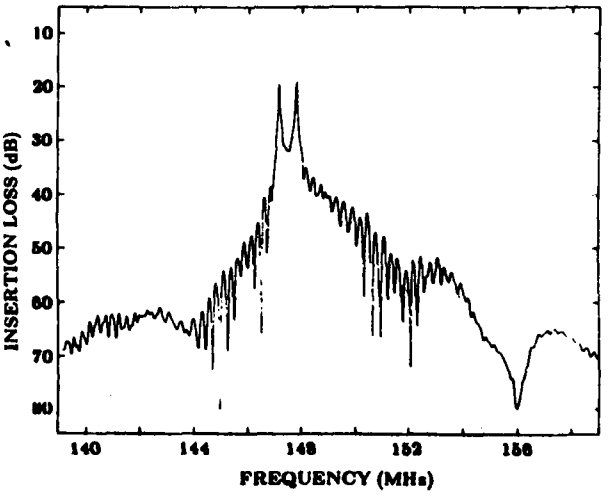

Fig. 7. Frequency response of a mode conversion resonator; λ_R=19.5 μm, λ_S= 35.0 μm, d=12.7 μm.

VII. Conclusion

Using design considerations which account for the dispersive nature of the layered medium, high-Q, temperature stable SAW resonators may be fabricated on silicon. Moreover, the favorable ageing rates obtained over the initial 30 day period following hermetic packaging indicates the feasibility of using resonators on silicon for commercial applications. In addition, the demonstration of resonators using two propagating modes indicates the possibility of constructing devices with enhanced rejection.

The authors would like to thank Dr. R. Razouk and L. Lie of Fairchild Corp. for preparing thick SiO_2 samples, and G. McGee of the Naval Avionics Center for making photomasks. This work was sponsored jointly by AFOSR grant AF810214 and NSF-MRL grant 8020249.

References

1 E. A. Ash, "Surface Acoustic Wave Grating Reflectors and Resonators," IEEE Symposium on Microwave Theory and Techniques, Newport Beach, Ca., May 11-14, 1970.

2 E. J. Staples, J. S. Schoenwald, R. C. Rosenfeld, and C. S. Hartmann, "UHF Surface Acoustic Wave Resonators," *1974 Ultrasonics Symposium Proc.*, IEEE Cat. No. 74 CHO 896-ISU, p. 245.

3 S. J. Martin, R. L. Gunshor, and R. F. Pierret, "Zinc-Oxide-on-Silicon Surface Acoustic Wave Resonators," Appl. Phys. Lett., **37**, p. 700, 1980.

4 S. J. Martin, R. L. Gunshor, and R. F. Pierret, "High-Q, Temperature Stable ZnO-on-Si SAW Resonators," *1980 Ultrasonics Symposium Proc.*, IEEE Cat. No. 80CH1622-1, p. 113.

5 S. J. Martin, S. S. Schwartz, R. L. Gunshor, and R. F. Pierret, "Surface Acoustic Wave Resonators on a ZnO-on-Si Layered Medium," to be published in J. Appl. Phys., Feb. 1983.

6 L. Storch, "The Transmission Matrix of N Alike Cascaded Networks," A.I.E.E. Trans., Part I, **73**, p. 616, 1955.

7 S. Datta and B. J. Hunsinger, "First-Order Reflection Coefficient of Surface Acoustic Waves from Thin-Strip Overlays," J. Appl. Phys., **50**, (9), p. 5661, 1979.

8 B. A. Auld, "Acoustic Fields and Waves in Solids," Vol. 2, John Wiley and Sons, New York, 1973.

9 R. L. Gunshor, S. J. Martin, and R. F. Pierret, "Surface Acoustic Wave Devices on Silicon," 1982 International Conference on Solid State Devices, Tokyo, Proceedings supplemental to Jap. Jour. of Appl. Phys., Jan. 1983.

10 T. Shiosaki, T. Yamamoto, and A. Kawabata, "Higher Order Mode Rayleigh Waves Propagating on ZnO/Substrate Structures," *1977 Ultrasonics Symposium Proc.*, IEEE Cat. No. 77CH1264-ISU, p. 814.

11 M. R. Melloch, R. L. Gunshor, and R. F. Pierret, "Conversion of Sezawa to Rayleigh Waves in the ZnO-SiO_2-Si Configuration," *1981 Ultrasonics Symposium Proc.*, IEEE Cat. No. 81CH1689-9, p. 765.

APPENDIX E

Presented at the Frequency Control Symposium, June 1983

SURFACE WAVE RESONATORS ON SILICON

S. J. Martin, R. L. Gunshor, T. J. Miller, S. Datta, R. F. Pierret
School of Electrical Engineering, Purdue University, West Lafayette, IN 47907

and

M. R. Melloch
Central Research Labs, Texas Instruments Inc., Dallas, TX 75265

INTRODUCTION

Over the past few years a development effort has been undertaken to adapt the surface acoustic wave (SAW) resonator to a silicon based configuration. The motivation for using silicon as the substrate lies in the possibility of incorporating SAW resonators in monolithic integrated circuits. The ZnO-on-Si two port resonator configuration, shown in Fig. 1, utilizes a thermally oxidized silicon substrate on which a piezoelectric ZnO layer is deposited to permit surface wave excitation. Surface features include aluminum interdigital transducers as well as distributed reflector arrays which are formed from grooves ion beam etched in the ZnO layer. An aluminum underlayer is deposited prior to ZnO sputtering. This underlayer serves to enhance the electromechanical coupling, in addition to isolating charge carriers in the semiconductor substrate from electric fields originating in the ZnO layer.

Two port SAW resonators fabricated on silicon have achieved Q-values of 12,000 at 100 MHz. Reflector arrays, formed by modulating the ZnO layer thickness with etched grooves, have been characterized by a linear change in reflectivity and wave velocity with groove depth[1]. Rejection levels of 30 dB have been obtained in devices with an untuned resonant insertion loss of 9 dB. An attractive feature results from the fact that the thermal expansion coefficient of SiO_2 is opposite in sign to that of Si and ZnO; it is possible to use the thermal oxide layer to temperature compensate the layered acoustic medium. The temperature stability of ZnO-on-Si SAW resonators has been shown to be comparable to those fabricated on ST quartz when the SiO_2 thickness is properly chosen[2]. To complement the temperature stability, a preliminary ageing study of hermetically packaged resonators has indicated that ageing rates of less than 5 ppm per month are obtainable.

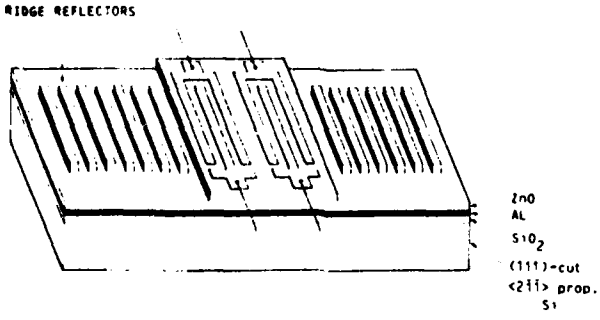

Fig. 1. SAW two-port resonator configuration using a piezoelectric ZnO layer on a thermally oxidized Si substrate.

In this paper we will discuss two topics new to the ZnO-on-Si resonator development:

1) The use of SAW resonators to determine the effect of a laser anneal on layered medium propagation loss.

2) A conceptually new device, called the mode conversion resonator, which utilizes two propagating normal modes of the layered medium in order to gain enhanced out-of-band signal rejection.

LASER ANNEALING OF THE LAYERED MEDIUM

A fundamental limitation on the Q-value achievable by a SAW resonator is set by the surface wave propagation loss. In the ZnO-SiO_2-Si layered medium, propagation loss is believed to dominate in the polycrystalline ZnO layer as evidenced by an increase in attenuation with ZnO thickness. A correlation has been found between the density of defects in the sputtered ZnO film and the propagation loss observed[3]. These defects, while much smaller than an acoustic wavelength, apparently act as Rayleigh wave scattering centers.

By using a ZnO layer on an oxidized Si substrate as an optical waveguide, Hickernell has suggested that optical propagation loss is dominated by defects located at the ZnO-SiO_2 interface. It was conjectured that these interface defects, arising during the initial stages of ZnO sputter-deposition, may also contribute significantly to surface wave attenuation. Attempts were made to reduce defects in the ZnO film through furnace annealing treatments. A decrease in tensile stress, as well as increased crystallographic ordering

revealed microfractures formed during the anneal. The accumulation of microfractures in successive scans at laser power densities above 10^5 W/cm^2 seems to cause wave scattering leading to Q-degradation. This observed effect of a laser anneal at excessive power levels might have been anticipated, since Hickernell has reported bulk recrystalization and micro-fracture formation in ZnO films subjected to furnace anneals at temperatures between 500-700° C.

At the optimum laser annealing power density, the decrease in acoustic propagation loss is less dramatic than that observed for optical prepagation loss by Dutta *et al.* It is conjectured that optical waveguiding, which relies on reflection at the upper and lower ZnO surfaces to confine light energy, may be more sensitive to defects at the ZnO-SiO_2 interface than is SAW propagation. SAW devices operating at higher frequencies and having a greater proportion of acoustic energy in the vicinity of the ZnO-SiO_2 interface may be more sensitive to interface defects. Such devices may benefit more from a laser anneal than those tested. Alternatively, propagation loss may not be the dominant source of loss in the resonant cavity. If other sources dominate losses, the improvement in propagation characteristics would not be fully reflected in the Q-value increase.

MODE CONVERSION RESONATOR

The second new development in ZnO-on-Si resonators which we address here is the operation of the mode conversion resonator. The devices discussed previously are constructed on a layered medium having a ZnO layer which is made as thin as possible in order to minimize surface wave attenuation. Consequently, only the lowest order sagittal mode (the Rayleigh mode) will propagate, as is the case at the surface of a semi-infinite homogeneous medium. When the ZnO layer is made sufficiently thick in relation to acoustic wavelength, it is possible to excite a second order sagittal mode or Sezawa mode.

In Fig. 4 the solid lines indicate the dispersion characteristics for Rayleigh and Sezawa modes propagating in a forward direction in a layered medium designed to support both modes. By using a periodic array of metal strips or grooves, it is possible to couple these forward modes into backward modes (indicated by dashed lines in Fig. 4) at points where the forward and backward branches intersect. The dispersion characteristics indicate the possibility of constructing a mode-converting reflector array. At ω_{RS} an incident Rayleigh mode R_+ is coherently scattered into a backward Sezawa mode S_-, and *vice versa*. The wavenumbers of the Rayleigh and Sezawa waves which participate in this reflection between modes must satisfy the relation

$$k_R + k_S = \frac{2\pi}{d} \qquad (1)$$

in which d is the mode conversion reflector periodicity. A resonant cavity may be formed between two mode-converting reflector arrays. A Rayleigh wave traversing the resonant cavity in one direction will be reflected as a Sezawa wave at the same frequency, provided Eq. 1 is satisfied. After traversing the resonant cavity in the opposite direction as a Sezawa wave, it will be re-reflected as a Rayleigh wave. A resonance condition is satisfied whenever the round trip phase shift is a multiple of 2π, i.e.,

$$\left(k_R + k_S\right)L_{eff} = 2n\pi \qquad (2)$$

where L_{eff} is the effective cavity length of the device and n is the longitudinal mode index. The transducers forming input and output ports are designed to couple energy into the resonant cavity in one propagating mode and out of the cavity from the other. As indicated in Fig. 5, one transducer having periodicity λ_R is positioned to couple optimally to the Rayleigh wave, while a second transducer, having periodicity λ_S, is placed to couple optimally to the Sezawa wave. The difference in transducer periodicities ensures a significant reduction in direct acoustic coupling between transducers, thereby inreasing the rejection level of the resonator. In designing transducers to couple to each mode, it is necessary to have appreciable electromechanical coupling to both modes with a given ZnO thickness. This condition is best achieved by placing transducers at the ZnO-SiO_2 interface,

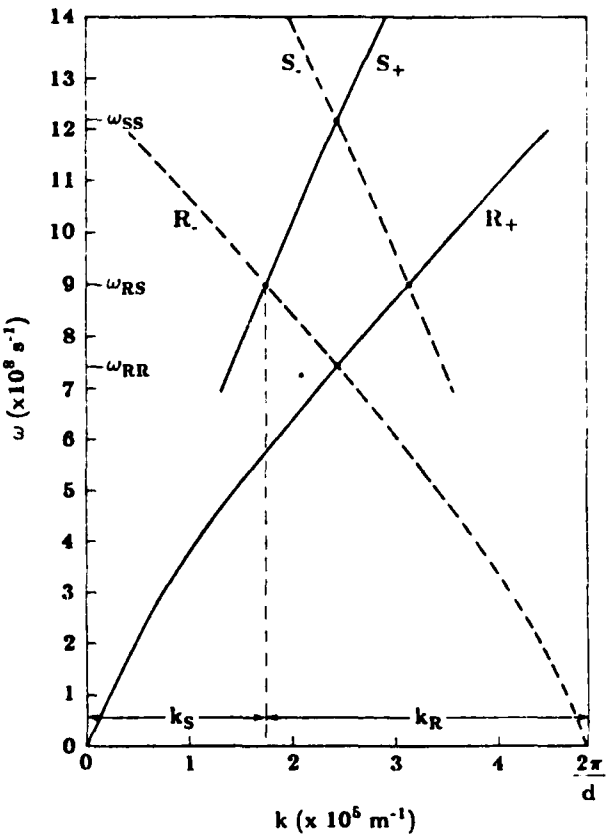

Fig. 4. Dispersion diagram illustrating Rayleigh and Sezawa mode propagation characteristics in a layered medium consisting of 6.5 μm ZnO on 1.0 μm SiO_2 on (100)-cut, <010>-propagating Si.

were observed in films annealed at 400° C[4]. However, no change was obtained in either optical or acoustic propagation loss.

On the other hand, annealing methods which provide localized heating at the ZnO-SiO_2 interface at a level which reduces defects were found to be successful in decreasing optical propagation loss. By exposing the substrate side of ZnO-on-Si optical waveguides to the radiant energy of a strip heater, in a process called "rapid isothermal annealing," Hickernell was able to reduce optical propagation loss by a factor of two[5].

An alternative means of providing localized heating was to use laser illumination in the infra-red region of the spectrum. At a laser wavelength of 10.6 μm ZnO and Si are nearly transparent, while the SiO_2 layer absorbs strongly. As shown by the laser absorption profile in Fig. 2, front side IR illumination of the layered medium provides localized heating at the ZnO-SiO_2 interface, precisely at the location where the defect density is believed highest. Dutta *et al.*[6] found that by laser scanning optical waveguides at power densities of approximately 2 x 10^5 W/cm^2 at a scan rate of 1 cm/sec, one could achieve a reduction in optical propagation loss of one to two orders of magnitude.

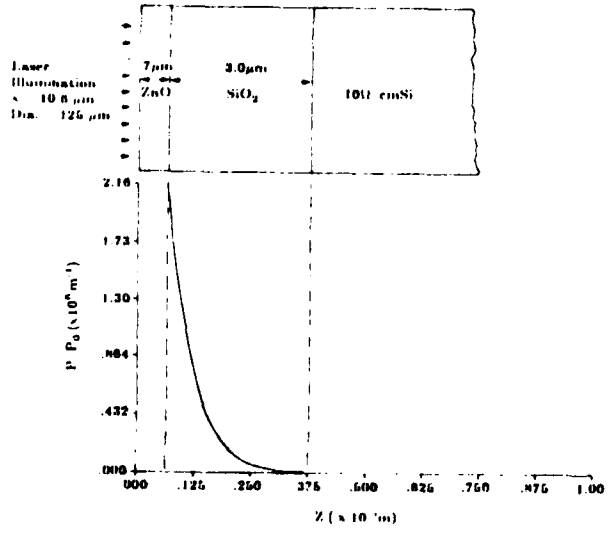

Fig. 2. Absorption profile of the incident CO_2 laser energy in the ZnO-SiO_2-Si layered medium. Defects at the ZnO-SiO_2 interface are reduced by the localized heating.

In both the rapid isothermal annealing experiment and the laser annealing experiment outlined above, experiments in which significant reductions in optical propagation loss were found, the experimenters did not determine the effect on acoustic propagation loss. It was our intention to use resonators fabricated on the ZnO-SiO_2-Si layered medium as a sensitive means to detect changes in acoustic loss caused by the laser anneal. The resonators employed in the experiment were fabricated on (111) Si, using a 3 μm SiO_2 layer and 0.75 μm ZnO layer. The 3 μm SiO_2 layer provides sufficient electrical isolation of the substrate from the ZnO electric fields so that an aluminum underlayer is not required for this purpose. In addition to eliminating transducer losses from the cavity, placing the transducers outside the resonant cavity enables one to eliminate aluminum from the region to be scanned. (Aluminum has proven detrimental in high temperature steps, diffusing into the ZnO layer and increasing the bulk conductivity.) By minimizing all sources of loss, these externally coupled resonators exhibited Q values of up to 14,000 at 100 MHz.

A CO_2 laser was used to scan the surface of each externally coupled resonator. A scanning apparatus containing an xy-translator was constructed to enable the stationary laser beam to raster-scan the surface of the device at a rate of 1 cm/sec. The scanner was capable of accomodating the device mounting case so that center frequency f_c and Q could be measured immediately before and after the laser scan at each power level. Placing the device 39 cm behind the lens (having a focal length of 40 cm) produced a spot size with a diameter calculated to be 0.125 mm.

The variation in resonant frequency and Q-value found after the laser anneal of a single device at successively higher laser power densities is shown in Fig. 3. We note a 3% maximum increase in Q-value after annealing at a laser power

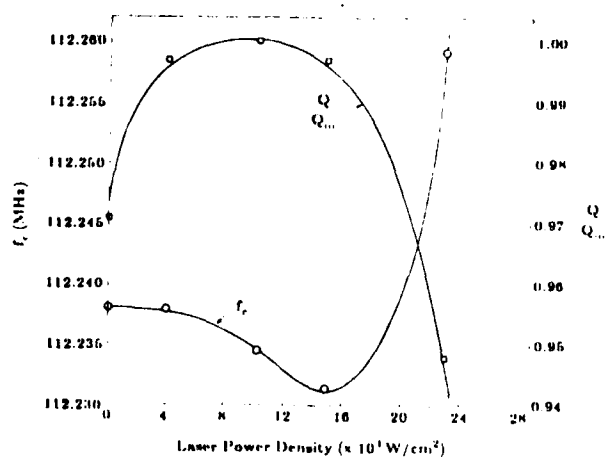

Fig. 3. Variation in resonant frequency and Q-value after laser annealing a single externally coupled resonator at successively higher power densities.

density of 9 x 10^4 W/cm^2. This power level is 42% of the value reported for optimum optical loss reduction. As our devices used a greater thickness of SiO_2 (3 μm as opposed to 1 μm), a greater efficiency is expected for localized heating. Thus the slight improvement in Q-value is attributed to a decrease in surface wave propagation loss through a reduction in interface defects. At higher laser power densities we note a rolloff in Q-value and a marked increase in resonant frequency. Microscopic examination of the device surface

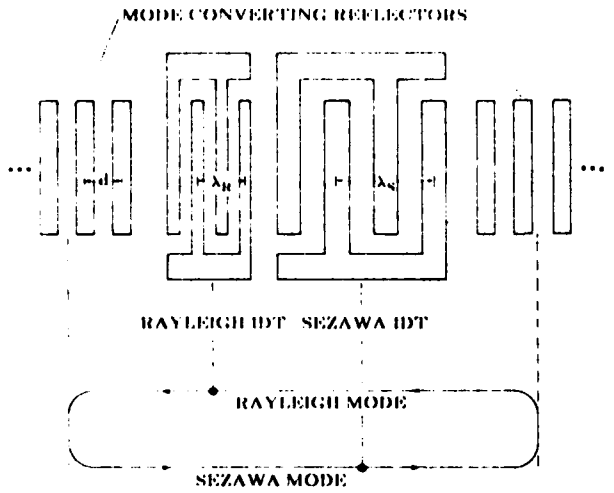

Fig. 5. Schematic of SAW mode conversion resonator. Input and output ports are tuned to different propagating modes, with distributed arrays coherently scattering between modes.

and employing a ground plane on top of the ZnO. Using a ZnO thickness of 6.5 μm and an SiO_2 thickness of 1.0 μm on (100)-cut <010>-propagating Si, the following values of electromechanical coupling were calculated: $\Delta_R = 0.016$, $\Delta_S = 0.021$.

In order to use a single masking step to simultaneously define IDT's and mode conversion reflector arrays, the array grooves were etched to a depth of 0.1 μm in the SiO_2 layer prior to the deposition of ZnO. The frequency reponses for two prototype mode conversion resonators are shown in Fig. 6 and Fig. 7. The device whose characteristics are shown in Fig. 6 exhibits two resonances. The large separation between mode converting arrays ($52\lambda_R$ or $29\lambda_S$), along with the detuning of resonance from the mode-conversion center frequency, causes Eq. 2 to be satisfied twice within the mode conversion bandwidth of the arrays. The out-of-band acoustic coupling level is seen to fall off more rapidly than that calculated for transducers tuned to the same propagating mode. Employing a smaller separation between mode-converting arrays ($32\lambda_R$ or $18\lambda_S$), the device whose characteristics are shown in Fig. 7 exhibits a single resonance peak. Due to the smaller number of transducer fingers, however, the rolloff in out-of-band acoustic coupling between transducers is less dramatic in this case.

Mode conversion resonator Q-values ranging from 2300 to 3000 have been obtained, indicating that power conversion efficiency between Rayleigh and Sezawa modes can exceed 90% with a 400-period array. In fact, device Q is thought to be limited primarily by propagation loss occurring in the 6.5 μm-thick ZnO film.

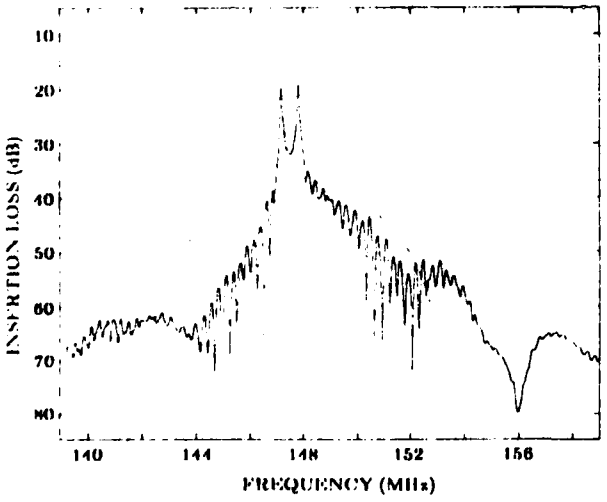

Fig. 6. Frequency response of a two-port mode conversion resonator. The calculated direct coupling level between transducers tuned to a single propagating mode is indicated by the dashed curve.

ACKNOWLEDGEMENT

This work was sponsored jointly by the Air Force Office of Scientific Research under grant AFOSR810214 and by the National Science Foundation under grant 8020249.

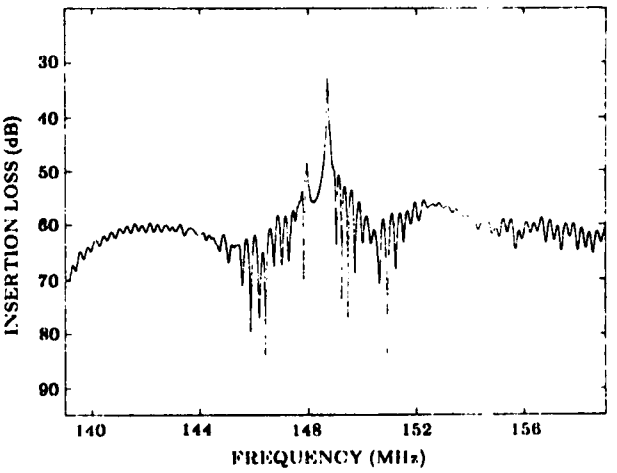

Fig. 7. Frequency response of a two-port mode conversion resonator exhibiting a single resonance peak.

REFERENCES

1. S. J. Martin, S. S. Schwartz, R. L. Gunshor, and R. F. Pierret, "Surface Acoustic Wave Resonators on a ZnO-on-Si Layered Medium," J. Appl. Phys., **54**, 561 (1983).
2. S. J. Martin, R. L. Gunshor, and R. F. Pierret, in *1980 Ultrasonics Symposium Proceedings*, (IEEE, New York, 1980) 113.
3. F. S. Hickernell, "Surface Acoustic Wave Propagation Loss in Zinc Oxide Films," in *1982 Ultrasonics Symposium Proceedings*, (IEEE, New York, 1982).
4. Ibid.
5. F. S. Hickernell, "Post Deposition Annealing of Zinc Oxide Films," in *1982 Ultrasonics Symposium Proceedings*, (IEEE, New York, 1981) 489.
6. S. Dutta, H. E. Jackson, J. T. Boyd, F. S. Hickernell, and R. L. Davis, "Scattering Loss Reduction in ZnO O[illegible]al Waveguides by Laser Annealing," Appl. Phys. Lett., **39**, 206 (1981).

APPENDIX F

Surface acoustic wave mode conversion resonator

S. J. Martin, R. L. Gunshor, M. R. Melloch,[a] S. Datta, and R. F. Pierret
School of Electrical Engineering, Purdue University, West Lafayette, Indiana 47907

(Received 13 December 1982; accepted for publication 16 May 1983)

It is well known that a ZnO-on-Si structure supports two distinct surface waves, called the Rayleigh and the Sezawa modes, if the ZnO layer is sufficiently thick. Herein we report a unique surface wave resonator that operates by efficiently converting between the two modes at the resonant frequency. The mode conversion resonator promises enhanced out-of-band signal rejection since input and output coupling is effected through different modes.

PACS numbers: 43.35.Pt, 43.88.Fx

In this letter we describe a conceptually new surface acoustic wave resonator in the ZnO-on-Si device configuration which employs mode conversion instead of simple reflection[1,2] to form a high Q resonant cavity. The conversion occurs between two propagating modes which are coupled through distributed mode-converting arrays. The proposed device offers potential advantages for improving out-of-band signal rejection in narrow band filters and resonators. Of particular interest is the high efficiency of mode conversion revealed by the experimental Q values exhibited by the device.

The layered acoustic medium formed by depositing a low velocity layer on a higher velocity substrate supports propagating surface acoustic modes in a manner analogous to the electromagnetic dielectric waveguide. The acoustic surface modes of interest are elliptically polarized with particle displacement confined to the sagittal plane and with amplitude decaying into the substrate in a manner similar to Rayleigh waves in a semi-infinite single material. The modes under consideration can be excited by means of an interdigital transducer placed either on top of the ZnO layer or between this layer and the SiO_2-Si substrate.[3]

The propagation characteristics for a particular layered configuration supporting two surface modes are shown in the dispersion diagram of Fig. 1. The lowest order sagittal mode, also called the Rayleigh mode, has no cutoff wavelength. The second order sagittal mode, called the Sezawa mode, propagates when the wave number exceeds some critical value. The dashed lines in Fig. 1 indicate the dispersion curves for backward Rayleigh and Sezawa modes which may be coupled to forward modes by an array of periodicity d. At intersection points wave energy and momentum are conserved, allowing forward waves to be converted into backward waves. Thus, several surface wave scattering events may occur at a periodic perturbation of such a bimodal layered acoustic medium. At ω_{RR} an incident Rayleigh wave R_+ will be reflected as a backward Rayleigh wave R_-, while at ω_{SS} an incident Sezawa wave S_+ will be reflected as a backward Sezawa wave S_-. Conventional surface wave resonators are designed to resonate at ω_{RR} or ω_{SS}, reflecting either Rayleigh or Sezawa waves between distributed reflector arrays.

At ω_{RS} either of two events may occur, involving the coherent scattering from a forward mode of one type into a backward mode of the other type. We previously demonstrated this type of scattering between an incident Sezawa mode S_+ and a backward Rayleigh model R_- by an array of metal strips or grooves in the ZnO layer.[4,5] From Fig. 1 it is apparent that at the same frequency an incident Rayleigh wave R_+ is scattered into a backward Sezawa wave S_-. Thus, a mode-converting reflector is formed by an array of periodicity d satisfying the relation

$$k_R + k_S = 2\pi/d, \tag{1}$$

at a fixed frequency, where k_R and k_S are the wave numbers of the Rayleigh and Sezawa modes participating in the conversion, respectively.

In the surface wave resonator reported herein, a reso-

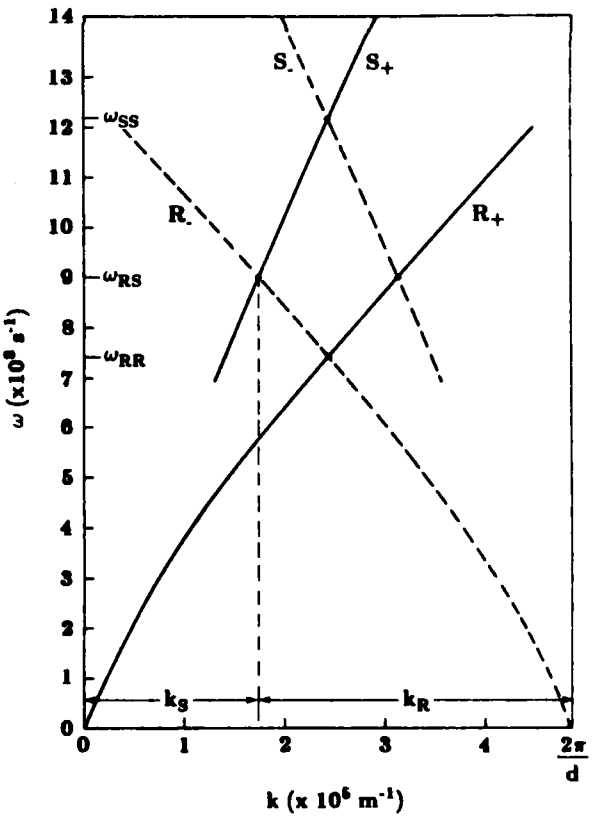

FIG. 1. Dispersion diagram illustrating Rayleigh and Sezawa mode propagation characteristics in a layered surface wave medium consisting of 6.5 μm ZnO on 1.0 μm SiO_2 on (100)-cut, (010)-propagating Si. Dashed lines indicate backward wave characteristics.

[a] Present address: Central Research Labs, Texas Instruments Inc., Dallas, TX 75265

 0003-6951/83/150238-03$01.00

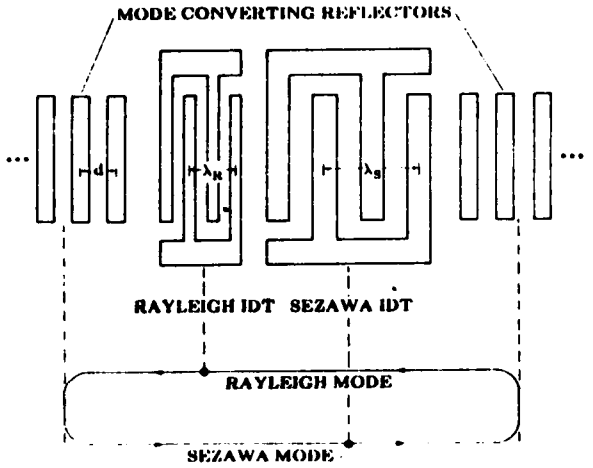

FIG. 2. Schematic of SAW mode conversion resonator. Input and output ports are tuned to different propagating modes with distributed arrays coherently scattering between modes.

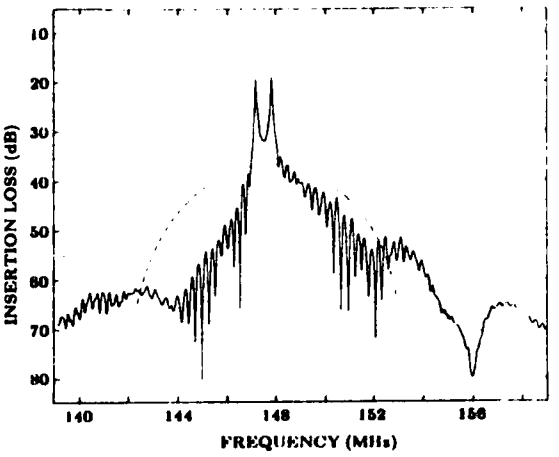

FIG. 3. Frequency response of a two-port mode conversion resonator. The calculated direct coupling level between transducers tuned to a single propagating mode is indicated by the dashed curve.

nant cavity is formed between two mode-converting reflector arrays, as shown in Fig. 2. A Rayleigh wave traversing the resonant cavity in one direction will be reflected as a Sezawa wave as detailed previously. After traversing the cavity in the opposite direction as a Sezawa wave, it will be re-reflected as a Rayleigh wave as indicated by the loop in Fig. 2. Wave energy is thus confined by alternately employing the scattering events at ω_{RS} rather than at ω_{RR} or ω_{SS}. A resonance condition is satisfied whenever the roundtrip phase shift—one way as a Rayleigh wave, one way as a Sezawa wave—is a multiple of 2π. This resonant condition may be expressed as

$$(k_R + k_S)L_{\text{eff}} = 2n\pi, \tag{2}$$

where n is the resonant longitudinal mode index and L_{eff} the effective cavity length of the resonator. Since bidirectional transducers are used, another loop having the opposite sense is excited; together these loops form simultaneous Rayleigh and Sezawa standing waves.

The transducers forming input and output ports are designed to couple energy into the resonant cavity in one propagating mode and out of the cavity from the other. One transducer having periodicity λ_R is positioned to couple optimally to the standing Rayleigh wave, while a second transducer, having periodicity λ_S is placed to couple optimally to the standing Sezawa wave. The difference in transducer periodicities ensures a significant reduction in direct acoustic coupling between transducers, thereby increasing the rejection level of the resonator.

In designing transducers to couple to each mode, it is necessary to have appreciable electromechanical coupling to both modes with a given ZnO thickness. Employing transducers on top of the ZnO yields high electromechanical coupling to the Sezawa mode Δ_S, but negligible coupling to the Rayleigh mode Δ_R. Transducers placed at the ZnO/SiO_2 interface, however, provide $\Delta_S = 0.024$ and $\Delta_R = 0.016$ with a ZnO thickness of 6.5 μm and SiO_2 thickness of 1.0 μm on a (100)-cut, ⟨010⟩-propagating Si substrate. A metal shorting plane is deposited on top of the ZnO to yield the values of coupling cited. In order to achieve a similar level of transducer static capacitance as well as radiation conductance, the number of finger pairs in the Rayleigh wave transducer is 1.6 times that of the Sezawa wave transducer.

In fabricating the mode-conversion resonator, aluminum transducers and mode-converting reflector grooves were defined on the SiO_2 layer in a single masking step. The grooves in the SiO_2 layer were ion-beam etched to a depth of approximately 0.1 μm. In addition to modulating SiO_2 thickness, the periodic grooves caused a corresponding topological variation on the surface of the subsequently deposited ZnO layer. This represents a departure from the previous practice of forming grooves on the top surface of the SAW propagation medium.[6,7] The net result of each period of this stacked perturbation is to scatter roughly 2% of the incident mode energy into a backward mode of the alternate type. At a frequency of 147 MHz a Rayleigh wave with $\lambda_R = 19.6$ μm is coupled to a Sezawa wave with $\lambda_S = 34.9$ μm by an array having periodicity $d = 12.9$ μm.

The frequency responses for two prototype mode conversion resonators are shown in Figs. 3 and 4. The device whose characteristics are shown in Fig. 3 exhibits two resonances. While a single resonance peak was desired, the large separation between mode converting arrays ($52\lambda_R$ or $29\lambda_S$), along with the detuning of resonance[8] from the mode-conversion center frequency, causes Eq. (2) to be satisfied twice within the mode-conversion bandwidth of the arrays. The mode conversion bandwidth is approximately 1.3 MHz. From the frequency separation of 0.64 MHz between resonances, we obtain an estimate of the effective cavity length: $L_{\text{eff}} = 148\lambda_R$ or $83\,\lambda_S$. We note that conventional resonators utilizing a single propagating mode may also exhibit multiple cavity modes. Each resonant cavity mode is comprised of contrapropagating Rayleigh and Sezawa modes, which together satisfy the periodic boundary conditions imposed at each end of the cavity by the mode-converting arrays. The nonresonant acoustic coupling level is seen to fall off rapidly away from resonance when compared with the direct coupling level calculated for transducers tuned to a single propagating mode.

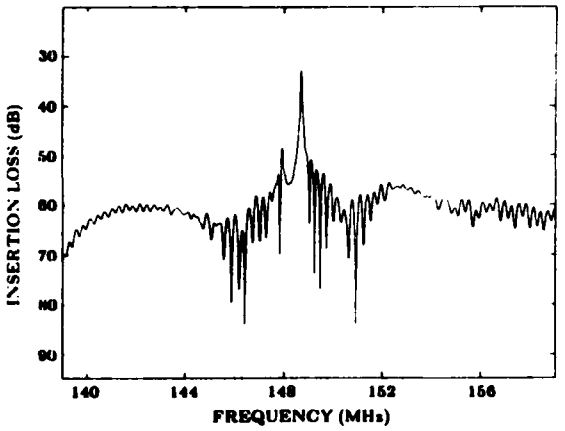

FIG. 4. Frequency response of a two-port mode conversion resonator exhibiting a single resonance peak.

Employing a smaller separation between mode-converting arrays ($32\lambda_R$ or $18\lambda_S$), the device whose characteristics are shown in Fig. 4 exhibits a single resonance peak. Owing to the smaller number of transducer fingers, however, the level of cross coupling (between Rayleigh transducer and Sezawa mode, Sezawa transducer and Rayleigh mode) is higher.

The off-resonance rejection of the mode conversion resonator could be enhanced by designing the transducers to minimize the level of cross coupling between transducers and propagating modes. The uniform transducers employed in the devices shown yield moderately high cross-coupling levels due to the sidelobes in the response characteristic.

Device Q values ranged from 2300 to 3000, indicating that power conversion efficiency between Rayleigh and Sezawa modes can exceed 90% with a 400 period array. In fact, device Q is thought to be limited primarily by propagation loss occurring in the 6.5-μm-thick ZnO film.

The authors would like to thank G. MaGee and S. Phillips of the Naval Avionics Center for help in making photomasks. This work was sponsored jointly by the National Science Foundation MRL program under grant 8020249 and by the Air Force Office of Scientific Research under grant AF810214.

[1] S. J. Martin, R. L. Gunshor, and R. F. Pierret, Appl. Phys. Lett. **37**, 700 (1980).
[2] S. J. Martin, R. L. Gunshor, and R. F. Pierret, in *1980 Ultrasonics Symposium Proceedings, Boston* (IEEE, New York, 1980), p. 113.
[3] M. R. Melloch, R. L. Gunshor, and R. F. Pierret, Appl. Phys. Lett. **37**, 147 (1980).
[4] M. R. Melloch, R. L. Gunshor, and R. F. Pierret, Appl. Phys. Lett. **39**, 476 (1981).
[5] M. R. Melloch, R. L. Gunshor, and R. F. Pierret, *1981 Ultrasonics Symposium Proceedings, Chicago* (IEEE, New York, 1981), p. 765.
[6] C. Dunrowicz, F. Sandy, and T. Parker, *1976 Ultrasonics Symposium Proceedings, Annapolis* (IEEE, New York, 1976), p. 386.
[7] W. J. Tanski, IEEE Trans. Son. Ultrason. **SU-26**, 93 (1979).
[8] S. J. Martin, S. S. Schwartz, R. L. Gunshor, and R. F. Pierret, J. Appl. Phys. **54**, 561 (1983).

APPENDIX G

UNIAXIALLY STRAINED $ZnO/SiO_2/Si$ SAW RESONATORS

Indexing terms: Ultrasonics, Surface-acoustic-wave devices, Resonators

Surface-acoustic-wave (SAW) resonators fabricated on a $ZnO/SiO_2/Si$ layered medium have been cantilever-mounted. By deflecting the free end of the substrate, uniaxial biasing strains are induced in the SAW resonator. The effect of these static strains on resonant frequency and SAW phase velocity is assessed.

The propagation of surface-acoustic waves (SAW) in a strained medium of such materials as quartz, lithium niobate or ZnO-on-quartz has been investigated in the past.[1,2] A significant portion of the recent studies is device-oriented, and deals specifically with the effect of an externally applied strain on the operating frequency of SAW delay-line or resonator oscillators. The extremely narrow bandwidth associated with high-Q SAW resonators, coupled with a strain dependence of resonant frequency, makes these devices particularly well suited for sensing displacement, force and pressure. By incorporating such sensors in an oscillator feedback loop, a strain-dependent frequency output is obtained which can readily be converted to digital form by a frequency counter.

Here we report the variation in resonant frequency with externally applied strain for resonators constructed on a $ZnO/SiO_2/Si$-layered medium. The measurements were carried out by deflecting a cantilever-mounted resonator as shown in Fig. 1. This method permits the resonant frequency, and ultimately the surface-wave phase velocity, to be expressed in terms of a single biasing strain in the direction of wave propagation.

The externally coupled SAW resonator employed here consists of input and output interdigital transducers (IDTs) lying outside a resonant cavity formed by two etched-groove reflector arrays. The functioning of the device is analogous to that of the optical Fabry–Perot cavity, with the exception that here the distributed reflectors have a narrow bandwidth. As a result of the reflector bandwidth, a single resonant mode exists and is characterised by a higher Q-value than would be obtained by placing transducers inside the resonant cavity. The device Q is 12 500 and is found to vary slightly with applied strain. This variation of Q is due in part to the velocity gradient which accompanies the nonuniform straining of the surface.

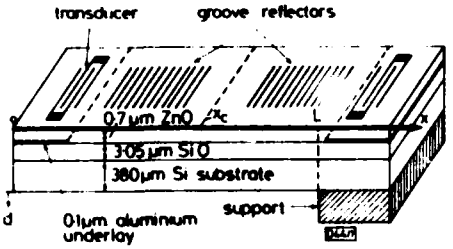

Fig. 1 *$ZnO/SiO_2/Si$ surface-acoustic-wave resonator mounted in cantilever fashion*

In fabricating the device, a thermal oxide is grown on a (111)-cut silicon substrate with wave propagation in the $\langle 2\bar{1}\bar{1}\rangle$ direction. Proper choice of SiO_2 thickness results in a temperature stable resonant frequency.[3] A piezoelectric ZnO film is deposited by RF diode or magnetron sputtering and permits transduction between the electrical signal and the propagating acoustic wave. The planar features on top of the ZnO are defined by standard photolithography, with reflector array grooves formed by ion-beam etching.

There are several advantages to using ZnO-on-Si SAW resonators as force/displacement sensing devices; these include:

(i) excellent mechanical properties, including high yield strength and low fatigue rate for highly polished, low defect density samples[4]

(ii) IC compatability, permitting integration of electronics along with sensing elements

(iii) the availability of preferential etches, delineated by doping characteristics, permitting the formation of thin membranes and intricate geometries[4]

(iv) the ability to vary turn-over temperature through SiO_2 thickness

(v) favourable ageing rates, on the basis of a recently reported preaging study.[5]

Deflection of the cantilever-mounted device results in an axial strain ε_x of opposing signs on the upper and lower surfaces. The SAW resonator, whose acoustic energy is confined to roughly one acoustic wavelength ($\lambda_0 = 40$ μm) of the top surface, and whose deposited layers are thin compared to substrate thickness, experiences essentially the strain occurring on top of the silicon.

Resonant frequency, which depends on both changes in propagation path length, as well as changes in phase velocity due to the biasing strain, deviates from the unstrained resonant frequency as

$$\frac{\Delta f}{f} = \frac{\Delta v}{v} - \frac{\Delta L_{eff}}{L_{eff}} \tag{1}$$

where L_{eff} is the effective cavity length of the resonator.

The biasing strain ε_x varies linearly in going from the deflected to fixed ends of the device so that the fractional change in effective cavity length is equal to the strain at the cavity centre, i.e. $\bar{\varepsilon}_x = \Delta L_{eff}/L_{eff}$. Measuring beam deflection d with a micrometer, the value of strain at cavity centre $\bar{\varepsilon}_x$ is given by[6]

$$\bar{\varepsilon}_x = \frac{3tx_c d}{2L^3} \tag{2}$$

where t is the total thickness of the substrate plus deposited layers and L is the unsupported beam length, as indicated in Fig. 1.

Resonant frequency is monitored during the strain test with an HP 8407A vector voltmeter. At each 0·001 in increment of beam deflection, applied at the free end of the device, input frequency from an HP 8656A signal generator is altered to restore the resonant phase shift between transducer ports. Owing to the rapid phase variation near resonance, transmission phase provides a more sensitive measure of detuning than does transmission amplitude. The variation in resonant frequency with biasing strain $\bar{\varepsilon}_x$ is shown in Fig. 2. From the linear characteristic, we can write $\Delta f/f = 1{\cdot}07\bar{\varepsilon}_x$. Using eqn. 1, with $\bar{\varepsilon}_x$ replacing $\Delta L_{eff}/L_{eff}$, we conclude that surface-wave velocity is influenced by biasing strain in the direction of propagation, such that $\Delta v/v = 2{\cdot}07\bar{\varepsilon}_x$. We note that the major effect of a strain in the direction of propagation is to increase surface wave velocity, resulting in a net increase in resonant frequency. In comparison, resonators fabricated on crystalline quartz or lithium niobate are found to decrease in resonant frequency with applied strain due to a smaller fractional change in surface-wave velocity with strain.[7,8]

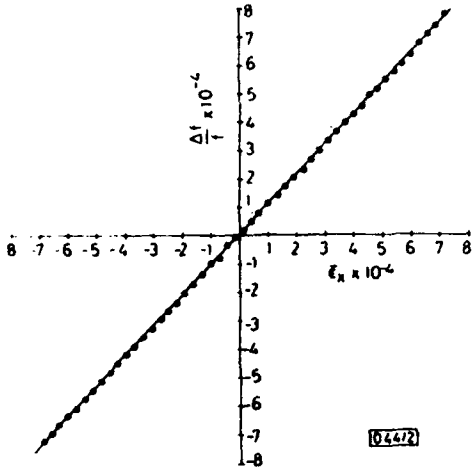

Fig. 2 *Variation in resonant frequency against strain at cavity centre in the direction of wave propagation*

In implementing a force sensor, crystal geometry governs the relationship between strain and applied forces. By using a thinner cantilever beam, for example, a greater threshold sensitivity is achieved. The threshold strain is that which produces the minimum resolvable resonant frequency shift. This is ultimately limited by the short-term frequency stability of the resonator. Short-term stabilities for quartz resonators are typically in the order of 1 Hz or less[10] (for integration periods of 1 s) with similar stability expected for resonators built on silicon.

It is found that resonant frequency of the $ZnO/SiO_2/Si$ devices varies linearly with applied strain up to the point of substrate fracture. Silicon yields by fracture, rather than by plastic flow, with maximum strain in the order of 10^{-3}. The dynamic range of a $ZnO/SiO_2/Si$ resonator sensor of any geometry will be limited by the ratio of maximum strain to threshold strain. On the basis of the measured maximum strain, and the estimated short-term resonator stability, the dynamic range of a 100 MHz sensor is estimated to be 10^5.

The authors would like to thank Dr. E. J. Staples of Rockwell International for performing the ageing study of resonators, S. Phillips and G. McGee of the Naval Avionics Center for making photomasks, and Dr. K. Tsubouchi of Tohoku University for several helpful discussions. This work was sponsored by AFOSR grant AF810214 and NSF-MRL grant 8020249.

12th October 1982

S. J. MARTIN
R. L. GUNSHOR
R. F. PIERRET

School of Electrical Engineering
Purdue University
West Lafayette, IN 47907, USA

G. GORODETSKY

Department of Physics
Ben-Gurion University
Beer-Sheva, Israel

References

1 SINHA, B. K., and TIERSTEN, H. F.: 'On the influence of uniaxial biasing stresses on the velocity of piezoelectric surface waves', 1976 Ultrasonics Symposium Proc., IEEE cat. no. 76 CH 1120-5SU, pp. 475–479
2 SALAMWAR, A. L., and EPSTEIN, M.: 'Surface acoustic waves in strained media', *J. Appl. Phys.*, 1976, **47**, pp. 43–48
3 MARTIN, S. J., GUNSHOR, R. L., and PIERRET, R. F.: 'High Q, temperature stable, ZnO-on-silicon SAW resonators', 1980 Ultrasonics Symposium Proc., IEEE cat. no. 80CH1622-1, pp. 113–117
4 PETERSEN, K. E.: 'Silicon as a mechanical material', *Proc. IEEE*, 1982, **70**, pp. 420–457
5 GUNSHOR, R. L., MARTIN, S. J., and PIERRET, R. F.: 'Surface acoustic wave devices on silicon'. 1982 International Conference on solid state devices, Tokyo, Proc. suppl. Jpn. J. Appl. Phys., Jan. 1983
6 TIMOSHENKO, S. P., and GOODIER, J. N.: 'Theory of elasticity' (McGraw-Hill, New York, 1970), Chap. 3, pp. 41–46
7 DIAS, J. F., KARRER, H. E., KUSTERS, J. A., and ADAMS, C. A.: 'Frequency/stress sensitivity of SAW resonators', *Electron. Lett.*, 1976, **12**, pp. 580–581
8 NALAMWAR, A. L., and EPSTEIN, M.: 'Strain effects in SAW devices', *Proc. IEEE*, 1976, **64**, pp. 613–615
9 REEDER, T. M., CULLEN, D. E., and GILDEN, M.: 'SAW oscillator pressure sensors'. 1975 Ultrasonics Symposium Proc., IEEE cat. no. 75 CHO 944-4SU, pp. 264–268
10 ROKHLIN, S. I., KORNBLIT, L., and GORODETSKY, G.: 'Analysis of surface acoustic wave pressure transducers and accelerometers'. Technical report, Physics, Materials Engineering Depts., Ben-Gurion University, Beer-Sheva, Israel

APPENDIX H

COMPARATIVE EVALUATION OF rf DIODE AND MAGNETRON SPUTTERED ZnO-SiO_2-Si STRUCTURES

R. D. Cherne, R. F. Pierret, and R. L. Gunshor
School of Electrical Engineering
Purdue University, W. Lafayette, IN 47907

M. H. Tanielian and O. K. Wu
Gould Laboratories
Gould Inc., Rolling Meadows, IL 60008

Abstract

A comparative evaluation of rf diode and magnetron sputtered ZnO-SiO_2-Si structures is described and summarized. The comparison incorporates both electrical data and physical data derived from SEM, X-ray diffraction, and other analytical techniques. The interfacial trap and net effective charge densities at the Si-SiO_2 interface, ZnO film morphology, ZnO film conductance, and the electrical and physical effects of post-deposition annealing are some of the topics examined in the comparison.

1. Introduction

Over the years rf diode sputtering, and more recently, rf magnetron diode sputtering have been the most widely utilized methods for depositing the ZnO film which forms the heart of metal-ZnO-SiO_2-Si (MZOS) device structures. Magnetron sputtering has tended to supplant non-magnetron rf diode sputtering (henceforth referred to as diode sputtering) because of an enhanced deposition rate and the routine attainment of thicker films of acceptable device quality. Another possible advantage of magnetron sputtering is reduced damage to the underlying Si-SiO_2 subsystem due to the decreased number of electrons bombarding the substrate during the deposition process.

Herein we summarize and report the results of a comparative evaluation of MZOS structures formed by diode and magnetron sputtering. The study was originally initiated to examine the relative levels of sputtering damage in the respective systems. Previous observations [1] of sputtering damage have been confined to the diode sputtering process and contained limited quantitative information. Further impetus for a comparative evaluation has come from observed differences in the electrical behavior of structures subjected to post-deposition annealing. As reported at the 1981 Ultrasonics Symposium [2], bias stable MZOS devices containing magnetron deposited ZnO films have been fabricated in our laboratory by annealing the ZnO-SiO_2-Si substrate in a nitrogen atmosphere for one hour at 380 - 490°C. The cited anneal, however, had no effect on the bias stability of MZOS devices containing diode sputtered films.

The majority of the data to be presented was derived from standarized structures with approximately 2μm thick ZnO films. The film in turn was typically deposited on (100) n-type Si substrates covered with a 0.1μm thick layer of thermally grown SiO_2. In examining the data it should be understood that the precise nature of the results is not only dependent on the device parameters, but is sensitive to even minute variations in the ZnO film deposition parameters and procedures (details of which are included elsewhere [3]). Overall trends, however, should be characteristic of the specific sputtering process, either diode or magnetron. The following section contains a review of representative sputtering damage observations. Physical observations including SEM, X-ray, and Auger data is presented in Section 3. A third distinct set of observations, results derived from small signal conductance measurements, are described in Section 4, while Section 5 contains an overall summary of results and conclusions.

2. Sputtering Damage Observations

The effect of radiation incuded damage on the Si-SiO_2 subsystem during sputter-deposition of an overlying ZnO film is most readily characterized in terms of (1) the density (D_{it}) of midgap surface states at the Si-SiO_2 interface and (2) the net effective interface charge per cm^2 (ΔQ_{SS}) added to the system during the deposition process. The midgap D_{it} provides a direct measure of the interface states created during sputtering. ΔQ_{SS}, computed from the flat band voltage of the system before deposition less the flat band voltage after deposition, is a combined measure of all charges added to the system. These typically include the positive charge associated with holes generated by ionizing radiation and trapped in the silicon dioxide near the Si-SiO_2 interface, added fixed charge, and changes in the interface state charge at flat band. Measured values of D_{it} before sputtering were less than 10^{10} states/cm^2-eV for the (100) oriented Si substrates employed in the investigation. ΔQ_{SS} was of course identically zero for an undamaged Si-SiO_2 subsystem.

Figs. 1 and 2 respectively display post-deposition D_{it} and $\Delta Q_{SS}/q$ values typical of MZOS structures formed by magnetron or diode sputtering. The x-axis on both plots identifies the position of the $Si-SiO_2$ substrate within the sputtering chamber during the deposition process. In collecting the data, a 3 inch $Si-SiO_2$ substrate was appropriately sectioned and the pieces positioned along a straight line through the center (x = 0) of the substrate platform as pictured in Fig. 3. After sputtering the ZnO film, the wafer pieces were further subdivided laterally and the upper halfs were post-ZnO-deposition (PZ) annealed at 380°C for one hour in an oxygen atmosphere.* MOS capacitors were then formed on all wafer pieces and probed as a function of position. The solid (●, ▲) data points appearing in Figs. 1 and 2 were derived from unannealed devices; the open (○,△) data points, from PZ annealed devices.

Several features of the damage produced during magnetron and diode sputtering are clearly evident from Figs. 1 and 2. First of all, the as-deposited (unannealed) damage is a strong function of the substrate positioning inside the sputtering chamber, with the positional dependence being especially pronounced for magnetron sputtering. In comparing the damage between various runs, or between magnetron and diode sputtering, it is absolutely essential to note the spatial positioning of the respective substrates on the substrate platform. Failure to note the spatial positioning can readily lead to confusing, seemingly irreproducible data, and possibly incorrect conclusions. Whereas lower minimum D_{it} values are obtained with magnetron sputtering, the overall damage is on the same order of magnitude for both sputtering methods.

Secondly, PZ annealing minimizes the spatial non-uniformity and drastically reduces the interface state density in highly damaged regions. However, the anneal has little effect on the midgap D_{it} in moderately damaged regions and, more importantly, a PZ anneal alone will not restore the $Si-SiO_2$ subsystem to pre-deposition quality. In fact, we have consistently observed a midgap D_{it} of $1\text{-}2 \times 10^{11}$ states/cm^2-eV in annealed magnetron structures compared to $<10^{10}$ states/cm^2-eV prior to sputtering.

Finally, although the midgap D_{it} is unaffected by the anneal for substrate positionings near x = 0, the ΔQ_{SS} of devices in this region increases after annealing. Since holes trapped in the oxide are undoubtedly removed by PZ annealing (which would tend to yield a negative shift in ΔQ_{SS}), the fixed charge is not affected by the anneal, and ionic contamination has

*This anneal was proposed in reference 1 as a means of minimizing the damage associated with sputtering.

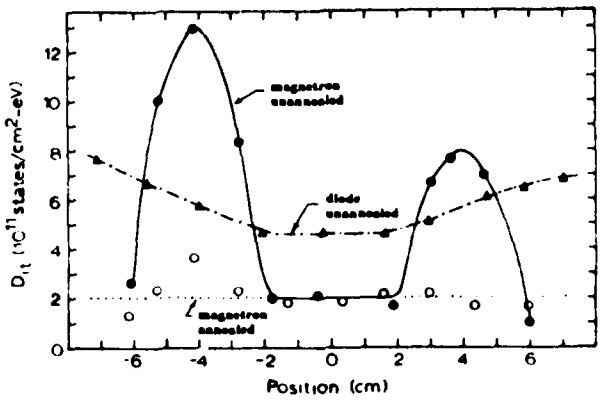

Fig. 1 Midgap interfacial trap density at the $Si-SiO_2$ interface as a function of substrate platform positioning.

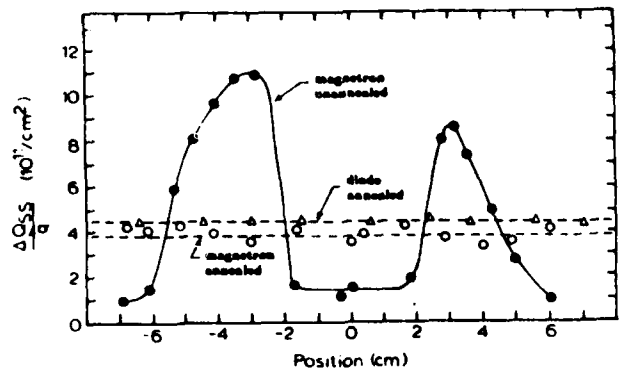

Fig. 2 Net effective interface charge per cm^2 at the $Si-SiO_2$ interface as a function of substrate platform positioning.

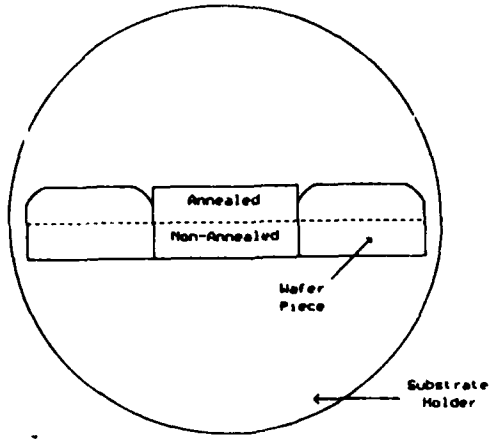

Fig. 3 Experimental arrangement of wafer pieces on the substrate platform leading to the data presented in Figs. 1 and 2.

been ruled out by subsidiary experiments, one can only conclude that the band edge distribution of acceptor-like and donor-like interface states is modified during the anneal. The uniformity of both D_{it} and ΔQ_{SS} after annealing also suggests the number and distribution of interface states are totally specified by the thermodynamic equilibrium condition established at the $Si-SiO_2$ interface during the annealing procedure.

3. Physical Observations

The primary motivation for performing a physical comparison of MZOS structures formed by magnetron and diode sputtering was the achievement of bias stability in PZ annealed magnetron structures but not in PZ annealed diode structures. Also of interest was the effect of the anneal on the physical nature of the ZnO films and the underlying $Si-SiO_2$ substrate. Thus, included in the analysis were magnetron-sputtered test structures, both annealed and unannealed, plus diode-sputtered test structures, both annealed and unannealed. The ZnO film in all cases was approximately 2μm thick and was deposited on a Si substrate covered with a ~0.1μm thick layer of thermally grown SiO_2. The PZ anneal was performed at 490°C for one hour in a nitrogen atmosphere. The test structures were eventually subjected to the following probes: scanning electron microscopy (SEM), X-ray diffraction (XRD), Auger depth profiling (AES), and electron spectroscopy for chemical analysis (ESCA).

As displayed in Figs. 4, the SEM analysis revealed that the magnetron films contained a coarser fiber morphology and a less regular columnar structure than the diode films. These results suggest a significantly larger grain size in the magnetron films and a more random growth pattern. PZ annealing appeared to have little effect on the gross morphology of the films, although the annealed samples did exhibit a somewhat increased surface roughness.

X-ray evaluation of the ZnO films was performed employing both a Read (powder) camera and an X-ray diffractometer. A qualitative comparison of the Read camera results again suggested that the magnetron films were not as well-oriented crystallographically as the diode films. The results further suggested that PZ annealing, and the attendant relaxation of stress in the ZnO films during annealing, enhanced the random orientation of crystallites--with the cited effect being decidely more pronounced for the magnetron films. The position of the 002 plane in the different ZnO films, as measured by the X-ray diffractometer, quantitatively confirmed the relaxation of film stress as a byproduct of PZ annealing. The measured 2θ values were 33.95°, 34.38°, 34.20° and 34.40° for the unannealed magnetron, annealed magnetron, unannealed diode, and annealed diode films,

(a)

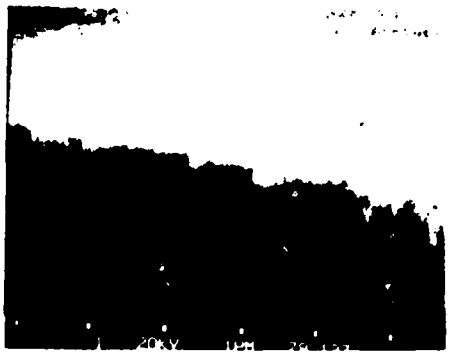

(b)

Fig. 4 SEM photographs of (a) magnetron sputtered and (b) diode sputtered ZnO films after PZ annealing. The spacing between hash marks is 1 μm.

respectively. By way of comparison, 2θ is ideally 34.43° for the 002 plane in an unstressed ZnO film. The degree of deviation from the ideal 2θ value clearly indicates considerable stress in the unannealed magnetron films and a significant reduction in stress upon annealing.

Auger depth profiling of the test structures established that the elemental composition of the ZnO film was uniform to within ± 2 atomic % throughout the thickness of the films. In all cases, profiles of the $ZnO-SiO_2$ and $Si-SiO_2$ interfaces were observed to be "smeared-out", which can be attributed in part to the intrinsic nature of the measurement technique and in part to uneven sputter-etching of the relatively thick ZnO layer. For both magnetron and diode structures, nonetheless the smearing out of the interfaces was enhanced after annealing as illustrated in Fig. 5. Unfortunately, it is not clear if intercomponent diffusion has actually occurred, or if this enhanced smearing is just an artifact caused

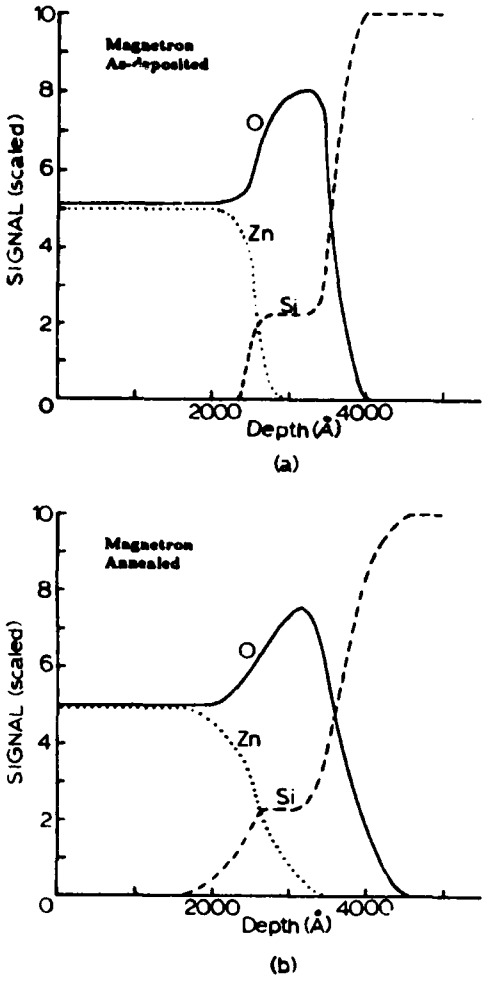

Fig. 5 Auger depth profile of the interfacial regions in a magnetron-sputtered MZOS structure (a) before and (b) after PZ annealing. (The zero point on the depth scale was chosen arbitrarily).

by the greater ZnO surface roughness of the annealed structures.

Finally, ESCA data indicated that, to within the accuracy of the measurement, zinc and oxygen were present in only one valence state each and that all films were stochiometric ZnO.

4. Small Signal Conductance Measurements

The small signal capacitance recorded as a function of voltage is a widely used tool for probing the internal properties of metal - insulator - semiconductor structures. C-V characteristics were, in fact, employed in establishing a portion of the data reported in Section 2. The admittance of all MIS structures, however, also exhibits a typically small but readily measurable loss component. Since the degree of bias stability exhibited by MZOS structures is intimately tied to carrier transport and trapping in the ZnO film, both of which contribute to the overall loss, it was felt that loss measurements might provide direct insight into the origin of behavioral differences displayed by magnetron and diode films.

The loss component, expressed in terms of the equivalent series resistance or equivalent parallel conductance, is generally a strong function of the a.c. measurement frequency and is therefore monitored as a function of both frequency and applied bias. For probing MZOS structures the capacitance and conductance measurements are complementary in nature. Whereas the constant capacitance portions of the C-V characteristics (corresponding to accumulation and inversion of the Si surface) provide only minimal structural information, the G-V and G-f characteristics are potentially rich in information over the same biasing regions. The observed conductance, on the other hand, is totally dominated by the Si-SiO_2 interface state loss under depletion biasing, thereby obscuring losses related to carrier transport and trapping in the ZnO film. For this reason, the conductance results to be reported are confined to the accumulation and inversion regions of operation. It should be noted that severe lateral effects under inversion biasing further restrict measurements performed with standard MZOS devices to only accumulation biases (to positive gate voltages for n-type devices). Inversion bias conductance data has nevertheless been obtained utilizing specialized "mesa" structures where the ZnO film is etched away in ungated areas.

Representative conductance versus frequency data derived from diode-sputtered MZOS-C's are displayed in Fig. 6. Other than predictable variations in magnitude associated with a square dependence on the device capacitance, the same results are obtained for all accumulating biases, all inverting biases, and whether the device is maintained in the dark or illuminated. Noting that the electric field distribution in the ZnO film is quite different under accumulation and inversion biasing, we are led to conclude the observed conductance has nothing to do with carrier transport and trapping in the ZnO film. The apparent lack of film photosensitivity, particularly under inversion biasing, further supports

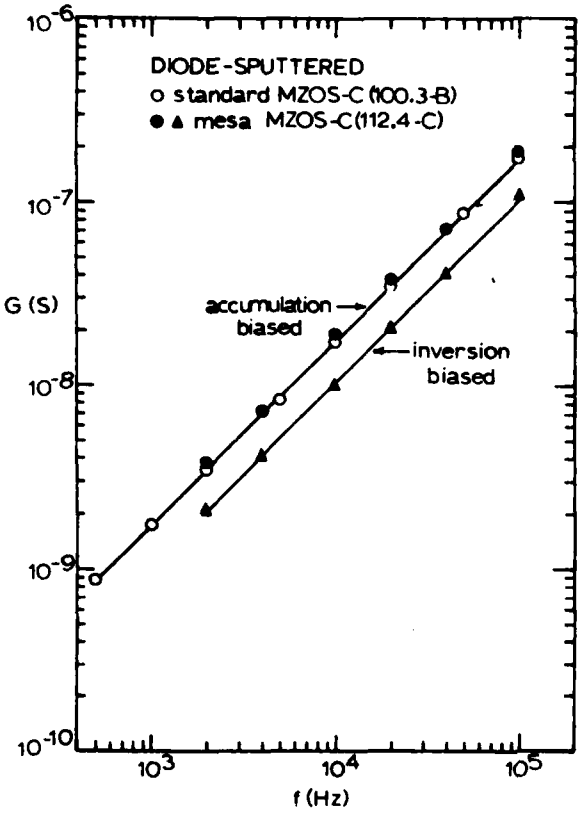

Fig. 6 (above) Representative conductance versus frequency data derived from diode-sputtered MZOS-C's.

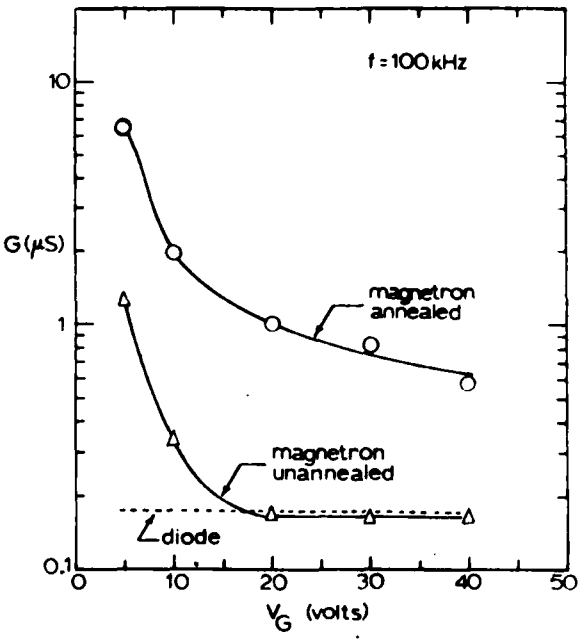

Fig. 7 (right-top), Observed conductance of magnetron MZOS-C's as a function of the applied gate voltage.

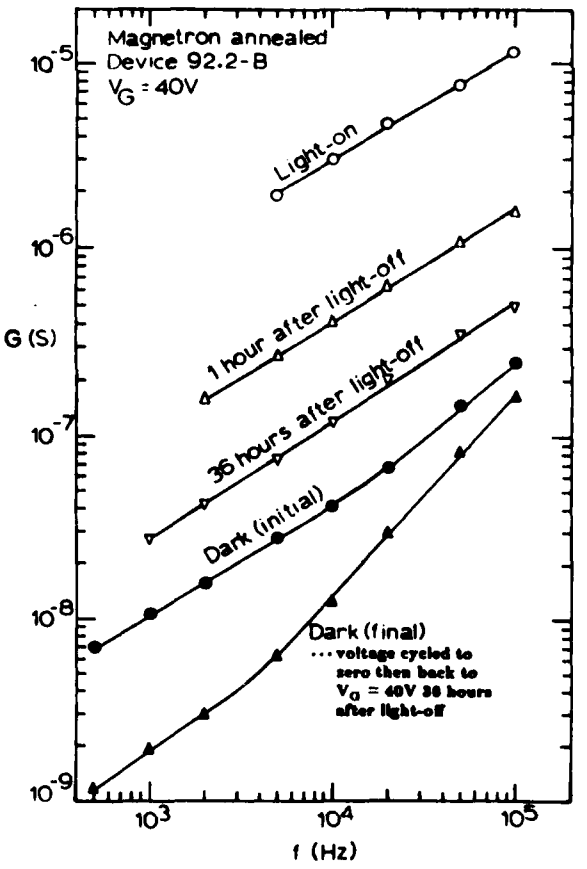

Fig. 8 (right-bottom) Conductance versus frequency characteristics of an annealed magnetron MZOS-C illustrating photo, memory, and voltage-history effects.

the cited conclusion. Additional measurements have in fact isolated the source of the observed loss to be the metal-ZnO contact. Absolutely no conclusions can be drawn about carrier conduction in the diode films, other than the film conductivity is below a certain calculable value.

Results derived from magnetron-sputtered MZOS-C's are decidely different. First of all, as displayed in Fig. 7, the measured conductance of magnetron devices is always greater than or equal to the conductance of comparable diode devices and only approaches the diode conductance at large accumulating biases. Secondly, illumination can increase the observed conductance of magnetron devices by orders of magnitude as shown in Fig. 8. Another interesting aspect of the Fig. 8

data is the persistence of a perturbed conductivity long after the illumination has been removed. Memory of a prior illumination, however, can be quickly erased by cycling the gate voltage from the set voltage to zero and then back again to the set voltage. Given the history and memory effects, it is our conclusion that the described behavior can be attributed to a high concentration of active upper band gap traps distributed throughout the bulk of magnetron-sputtered ZnO films. These traps are either absent in the diode films or present at lower concentrations. Finally, PZ annealing apparently leads to an increased trap density in the magnetron films.

5. Summary and Conclusions

In this paper we have presented a brief overview of results comparing the electrical and physical properties of MZOS structures formed in our laboratory by diode and magnetron sputtering. One major result was the observation that damage produced during sputtering was a function of the substrate positioning, with the spatial dependence being especially pronounced for magnetron sputtering. Magnetron sputtering gave rise to lower as-deposited damage for devices formed in the center of the substrate holder, but the overall sputtering damage was comparable for the two sputtering techniques. Although PZ annealing did not restore the $Si-SiO_2$ subsystem to pre-deposition quality, it drastically reduced the interface state density in highly damaged regions and essentially eliminated the spatial non-uniformity. A midgap $D_{it} = 1 - 2 \times 10^{11}$ states/cm^2-eV is considered representative of the residual damage in annealed magnetron structures.

Physical observations generally indicated the sputter-deposited films to be of SAW device quality. All films were confirmed to be oriented stochiometric ZnO with an elemental composition uniform to ±2 atomic percent throughout the thickness of the film. Magnetron films, however, were found to have a coarser fiber morphology and a less regular columnar structure. In addition, considerable compressive stress was detected in as-deposited magnetron films. PZ annealing led to a reduction in film stress, a somewhat increased surface roughness, and an enhanced smearing in the Auger profile of the component interfaces.

Finally, the measured small signal conductance derived from magnetron and diode-sputtered devices was distinctly different. The conductance of diode MZOS-C's was dominated by losses stemming from the metal-ZnO contact and provided little if any information about the ZnO film itself. The G-V and G-f characteristics derived from magnetron devices, on the other hand, were clearly correlated with carrier action inside the ZnO film. It was concluded from this data that the magnetron films contained a high density of upper band gap traps whose numbers are increased by PZ annealing. These same traps undoubtedly play a key role in the bias stability of annealed magnetron devices and may in fact arise as a direct consequence of the larger fiber morphology of the magnetron films.

Acknowledgment

The material presented in this paper is based upon work supported by the National Science Foundation under Grant No. ECS-8009793 and by the Air Force Office of Scientific Research under Grant No. AFOSR-81-0214.

References

1) M. E. Cornell, J. K. Elliott, R. L. Gunshor, and R. F. Pierret, Appl. Phys. Lett., 31, 560 (1977).

2) R. D. Cherne, M. R. Melloch, R. L. Gunshor, and R. F. Pierret, 1981 Ultrasonics Symposium Proceedings, p. 780 (IEEE, Chicago, 1981).

3) R. D. Cherne, "Electrical Characterization of MZOS Structures", Ph.D. Thesis, School of Electrical Engienering, Purdue University, Dec. 1982.

APPENDIX I

-to appear in J. Appl. Phys. (August 1983)

Space Charge Waves in Multilayered Heterostructures

S. Datta and R. L. Gunshor
School of Electrical Engineering
Purdue University
West Lafayette, IN 47907

ABSTRACT

Space charge waves in multilayered heterostructures are discussed using coupled Boltzmann equations. Acoustic plasma modes are investigated with practical examples. The formulation includes both degenerate and non-degenerate electron systems; exchange and correlation effects are incorporated using a local density approximation and are shown to affect the acoustic plasma mode significantly; lattice collisions are included using the relaxation time approximation.

1. Introduction.

The development of molecular beam epitaxy has made it possible to fabricate multiple layers (thickness ~100Å) of lattice-matched semiconductors with a very low density of interface states[1]. Various combinations of semiconductors have been used to build multilayered heterostructures, the most popular combination being GaAs and $Al_{1-x}Ga_xAs$ (Fig. 1a). The idealized conduction and valence band edges for such a configuration are shown in Fig. 1b. The electrons are confined in narrow gap GaAs layers where they are free to move in the x-y plane; the result is a series of potential wells, each well within which a system of two dimensional free electrons is confined.

Electrons confined in two dimensions support space charge waves that have a plasma frequency proportional to the square root of the wavenumber. In multilayered structures the space charge waves in different wells are coupled through the Coulomb interaction. The coupling of two distinct electron systems leads to the appearance of two modes - the optical plasma mode where the space charge waves in the two systems are in phase, and the acoustic plasma mode where they are out of phase. The latter mode type possesses interesting possibilities for application to practical devices; such modes exhibit an approximately linear frequency - wavenumber relationship with velocities of the order of 10^8 cm/second. This velocity range is about 3 orders of magnitude faster than ultrasonic waves, and 2 orders of magnitude slower than electromagnetic waves. It may thus be possible to use such acoustic plasma waves to implement

submillimeter wave signal processing components. The use of these plasma waves is limited on the low frequency side by the collisional damping of the lattice and impurities. However, modulation doping techniques have been reported that make it possible to obtain very long collision times (far in excess of the Brooks - Herring limit for bulk materials) in multilayered heterostructures[2]. Collision times in the range of 1 ps. would make acoustic plasma waves useable at frequencies in the 1000 GHz range.

Acoustic plasma modes were first discussed in three dimensional systems having two distinct species of electrons such as s-and d-electrons or electrons and holes[3,4]. However, acoustic plasma modes in these systems are Landau damped by the lighter species[5] and are difficult to observe. Collective modes of spatially separated two dimensional electron systems in solids were first investigated by Dassarma and Madhukar[6] using the Random Phase approximation (RPA) for the dielectric constant. They found that an acoustic mode exists even if the two systems are identical; moreover, if the spatial separation exceeds a certain critical value the mode is not Landau damped by either species.

In this paper we will present an analysis of the acoustic plasma modes in spatially separated two dimensional electron systems using coupled Boltzmann equations. The Boltzmann formalism is equivalent to the RPA for long wavelength excitations; so as we might expect, this analysis gives the same results as Ref. 6. However, the present formulation, we believe, is more suitable for further extending the analysis in order to

incorporate additional effects. The effects of correlation and exchange are incorporated using a local density approximation; both degenerate and non-degenerate (classical) systems are included in the analysis. The effect of collisions (with the lattice) is incorporated through a relaxation time τ. A similar formalism has recently been used to describe acoustic plasma modes in three dimensional systems with two species of electrons.[5]

2. Coupled Boltzmann Equations for a Pair of Wells

Consider a pair of wells (Fig. 1b) each of width W and separated by a distance d. In each well the electrons are distributed in different subbands depending on the width of the well, the carrier concentration and the temperature. We will assume for simplicity that only the lowest subband in each well is occupied, so that we have two groups of electrons, one in each well; however, electrons in multiple subbands can also be incorporated into the formalism in a fairly straightforward manner.

We have two species of two dimensional electrons spatially separated by d. Let $f_1(\vec{r},\vec{v})$ and $f_2(\vec{r},\vec{v})$ be the distribution functions, both $\vec{r}$ and $\vec{v}$ being in the x-y plane. We can write a set of coupled Boltzmann equations for f_1 and f_2:

$$\left[\frac{\partial}{\partial t} + \frac{1}{\tau} + v_i \cdot \nabla_r\right] \delta f_i - \sum_{j=1}^{2} \nabla_r V_{ij} \cdot \frac{\nabla_v f_i}{m_i^*} = 0, \quad i = 1,2,... \tag{1}$$

where $\delta f_i = f_i - f_i^o$

f_i^o = equilibrium distribution function

$\nabla_{r,v}$ = gradients in $\vec{r}$ and $\vec{v}$ space respectively

V_{ij} = potential at the location of electrons in system i,
arising from charge bunching in system j.

m_i^* = effective mass of electrons in system i.

Let us consider space charge waves with frequency ω and wavenumber $\vec{k}$; Equation (1) then becomes

$$\left[j\omega + \frac{1}{\tau} - j\vec{k}\cdot\vec{v}_i\right] \delta f_i + \sum_{j=1}^{2} j\vec{k}\cdot\vec{v}_i \, V_{ij} \frac{\partial f_i}{\partial E_i} = 0, \quad i = 1,2,... \tag{2}$$

where we have used $\vec{\nabla}_v f_i = m_i^* \vec{v}_i \frac{\partial f_i}{\partial E_i}$. Taking $\vec{k}$ as the reference direction in the x-y plane we can represent $\vec{v}_i$ by its magnitude v_i and its angle θ_i from $\vec{k}$. We then have from (2),

$$\delta f_i = - \frac{\partial f_i}{\partial E_i} \frac{k v_i \cos\theta_i}{\Omega - k v_i \cos\theta_i} \phi_i, \quad i = 1,2,... \tag{3a}$$

where $\Omega = \omega - j/\tau$, and

$$\phi_i = \sum_{j=1}^{2} V_{ij} \tag{3b}$$

The potentials V_{ij} are related to the excess carrier concentration δn_j by

$$V_{ij} = \frac{q^2}{2\epsilon k} \delta n_j \quad , \quad i = j \tag{4a}$$

$$= \frac{q^2}{2\epsilon k} e^{-kd} \delta n_j, \quad i \neq j \tag{4b}$$

where k is the magnitude of the wavenumber, d is the separation between wells, ϵ is the static dielectric constant and q is the electronic charge. Eq. (4) is derived from Poisson's equation, neglecting the spatial spread of the space charge in the z-direction

assuming that the charge forms a sheet in the x-y plane at the center of the well. The exchange and correlation effects can be included approximately in a local density approximation by modifying V_{ij} using the Slater coefficients[5]. The excess carrier concentration is related to the distribution function by

$$\delta n_j = \frac{m_j^{*2}}{2\pi^2\hbar^2} \int d\vec{v}\, \delta f_j \tag{5}$$

Using Equation (3a) in (5),

$$\delta n_j = \frac{m_j^{*2}}{2\pi^2\hbar^2}\, \phi_j \int_0^\infty dv_j \int_0^{2\pi} d\theta_j v_j\, \frac{k v_j \cos\theta_j}{\Omega - k v_j \cos\theta_j} \cdot \left[-\frac{\partial f_j}{\partial E_j}\right] \tag{6}$$

Using the result

$$\frac{1}{2}\int_0^{2\pi} \frac{\cos\theta}{\lambda - \cos\theta}\, d\theta = -1 + \frac{\lambda}{\sqrt{\lambda^2 - 1}}$$

$$\equiv g(\lambda)$$

we have from Equation (6),

$$\delta n_j = \phi_j N_j' \int_0^\infty dE_j\, g\left(\frac{\Omega}{k v_j}\right) \cdot \left[\frac{-\partial f_j}{\partial E_j}\right] \tag{7}$$

where $N_j' = \frac{m_j^*}{\pi\hbar^2}$ and represents a two dimensional density of states in the j^{th} band, while $E_j = \frac{1}{2} m_j^* v_j^2$

The integral in Equation (7) is evaluated using the equilibrium distribution function f_j^o for f_j. If the carrier concentration is high and the temperature is low such that $E_F \gg k_B T$ it is appropriate to set

$$-\frac{\partial f}{\partial E} \simeq \delta(E - E_F) \tag{8}$$

so that Equation (7) reduces to

$$\delta n_j = \phi_j \, N_j' \, g(\lambda_j) \tag{9}$$

where

$\lambda = \Omega / k v_{Fj}$

v_{Fj} = Fermi velocity of electrons in system j

A carrier density n of $10^{12}/cm^2$ (corresponding to a bulk density of $10^{18}/cm^3$ if $w = 100\mathring{A}$) gives

$k_F = \sqrt{2\pi n} = 2.5 \times 10^6 \text{ cm}^{-1}$

$v_F = 4.3 \times 10^7$ cm/s. $\quad (m^* = .068 \, m_o)$

$E_F = 35.8$ meV

Thus the approximation (8) is valid at low temperatures. The subband separation for $w = 100 \mathring{A}$ is about 56 meV so that the neglect of carriers in higher subbands is also justified.

If the carrier concentration is low and the temperature high enough, the Boltzmann distribution is more appropriate

$$-\frac{\partial f}{\partial E} = \frac{1}{k_B T} e^{-E/k_B T} \cdot \frac{n}{k_B T \cdot N'}$$

The constant has been chosen so that the integral of f over energy yields the correct carrier concentration n. We then have from (7),

$$\delta n_j = \phi_j \frac{n_j}{k_B T} g'(\lambda_j) \tag{10}$$

where

$$g'(\lambda_j) = \int_0^\infty dx\ e^{-x}\ g\left[\frac{\lambda_j}{\sqrt{x}}\right]$$

$$\lambda_j = \Omega / k v_{tj}$$

$$v_{tj} = \begin{matrix}\text{Thermal velocity of} \\ \text{electrons in system j}\end{matrix} = \left[\frac{2k_B T_j}{m_j^*}\right]^{1/2}$$

Equations (9) and (10) can be written together as

$$\delta n_j = \phi_j N_j F(\lambda_j) \tag{11}$$

where $F(\lambda_j)$ and N_j are defined by Equation (9) for degenerate system and by Equation (10) for a non-degenerate system. The intermediate case is more complicated algebraically since the exact Fermi-Dirac function has to be used for f(E).

Using Equation (11) in Equation (4) and substituting in Equation (3b) we have

$$\begin{bmatrix} 1 + \alpha_1 & \alpha_2 e^{-kd} \\ \alpha_1 e^{-kd} & 1 + \alpha_2 \end{bmatrix} \begin{Bmatrix} \phi_1 \\ \phi_2 \end{Bmatrix} = \begin{Bmatrix} 0 \\ 0 \end{Bmatrix} \tag{12a}$$

where

$$\alpha_i = - \frac{q^2}{2\epsilon k} N_i F(\lambda_i) \tag{12b}$$

The plasma modes of the coupled wells are obtained from the condition

$$\det \begin{bmatrix} 1 + \alpha_1 & \alpha_2 e^{-kd} \\ \alpha_1 e^{-kd} & 1 + \alpha_2 \end{bmatrix} = 0 \tag{13}$$

The present formalism is easily extended to multiple systems of electrons; it only makes the order of the matrix in Equation (13) larger. The α_i's are actually the

polarizabilities of the electrons in system i, so that the matrix in Equation (13) is really a generalized permittivity for the coupled system. If the off diagonal terms were absent, Equation (13) would give $1 + \alpha_1 = 0$ or $1 + \alpha_2 = 0$ which describes the plasma modes of the individual systems. But because of the coupling we now have

$$1 + (\alpha_1 + \alpha_2) + \alpha_1\alpha_2(1 - e^{-2kd}) = 0 \qquad (14)$$

The different space charge modes predicted by Equation (14) will be discussed in the next section. As we mentioned earlier, exchange effects can be approximately incorporated by subtracting an exchange potential V_{xc} from the V_{ij} (i=j) in Equation (4a); since the two systems are spatially separated, exchange does not affect the V_{ij} for $i \neq j$ (assuming there is no overlap in the wave functions). The exchange energy per electron U_{xc} can be estimated for a degenerate electron system using[8]

$$U_{xc} = -\int_{|\bar{K}'| \leq k_F} \frac{q^2}{2\epsilon|\bar{K} - \bar{K}'|} \frac{d\bar{K}'}{4\pi^2}$$

$$= -\frac{q^2}{2\epsilon k_F} n \quad @\ \bar{K} = 0,\ \bar{K} \text{ being the electron wavevector.}$$

A change in the electron density by δn produces a change in the exchange energy which can be approximately accounted for by an exchange potential

$$V_{xc} = -\frac{q}{2\epsilon k_F} \delta n.$$

For degenerate systems the effect of exchange is to reduce α_1 and α_2 appearing in the diagonal elements of Eqs. (12) and (13). This modifies Eq. (14) to

$$1 + \gamma(\alpha_1 + \alpha_2) + \alpha_1\alpha_2(\gamma^2 - e^{-2kd}) = 0 \qquad (16)$$

where

$$\gamma \simeq 1 - k/k_F$$

For long wavelength excitations γ is close to 1; but e^{-kd} is also close to 1 for small d. As we shall see, the frequency of the acoustic modes depends on the difference $(\gamma^2 - e^{-2kd})$, so that exchange effects could play a significant role in degenerate systems. Exchange effects are usually smaler in nondegenerate systems.

3. Acoustic Plasma Mode for Identical Wells

We will now discuss the acoustic plasma mode for a pair of wells; which are assumed identical. It will be shown that the acoustic mode is not Landau damped if the spacing d between the wells is large enough. Since the wells are identical we have

$$\alpha_1 = \alpha_2 = \alpha$$

From Equation (14),

$$\alpha = -(1 \pm e^{-kd})^{-1}$$

$$\simeq -\frac{1}{2} \text{ or } -\frac{1}{kd} \quad \text{if } kd \ll 1$$

The eigenvalue $\alpha = -1/2$ leads to the optical plasmon where space charge waves in the two wells are in phase; $\alpha = -1/kd$ corresponds to the acoustical plasmon where they are out of phase. The association between wave type and eigenvalue can be seen by considering the corresponding solutions ϕ_1, ϕ_2 in Equation (12a). For the acoustical plasmon,

$$\alpha kd = -1$$

that is,

$$\frac{2d}{L_D} = \frac{1}{F(\lambda)} \tag{17}$$

where L_D represents the screening distance for a degenerate electron system given by

$$L_D = \left[\frac{q^2 m^*}{4\pi\epsilon\hbar^2}\right]^{-1} = 79\text{Å}$$

if $m^* = .068\ m_o$, $\epsilon = 10\ \epsilon_o$ (typical values for GaAs). Let us assume that $\lambda >> 1$ so that the mode is not Landau damped. This means that the wave velocity is much larger than the Fermi velocity of the electrons (for degenerate systems) or their thermal velocity (for non degenerate systems). We then have

$$g(\lambda) \simeq 1/2\ \lambda^2$$

For degenerate systems one has $F(\lambda) = g(\lambda)$; for non-degenerate systems the integral in Equation (10) gives approximately the same resutl, so that we may set

$$\frac{1}{F(\lambda)} = 2 \cdot (\Omega/kv)^2 \tag{18}$$

with v equal to the Fermi velocity (v_F) for degenerate electrons and to the thermal velocity (v_t) for non-degenerate electrons. Using Equation (18) in (17),

$$\frac{\Omega}{k} = v \cdot \sqrt{\frac{d}{L_D}} \tag{19}$$

If $d >> L_D$, the mode velocity is much larger than v and the assumed condition of zero Landau damping is satisfied; however, we may still have collisional damping unless the frequency is high enough that $\omega >> 1/\tau$ (since $\Omega = \omega - j/\tau$).

Consider a potentially practical example. If $d = 1000\text{Å}$ and $n = 10^{12}/cm^2$, then for GaAs we have (assuming a degenerate system) $V_F = 4.3 \times 10^7$ cm/s.

$$\frac{\Omega}{k} = 3.6\, V_F = 1.55 \times 10^8 \text{ cm/s}.$$

At a frequency of 500 GHz, the wavelength is $\simeq 3.1\ \mu$m, so that interacting structures can be fabricated on the surface by photolithographic techniques. However, the design of transducers for these waves may prove difficult because of the necessity to excite two nearby wells having a 180° phase difference.

Finally, it should be noted that the velocity of the acoustic mode depends on the difference $1-e^{-kd}$ so that it might be significantly affected by exchange and correlation as mentioned at the end of the last section.

4. Conclusions

In this paper we have described a Boltzmann formalism for describing coupled space charge waves in spatially separated two dimensional systems as encountered in multilayered heterostructures. Both degenerate and nondegenerate electron systems can be handled by this formalism. Acoustic plasma modes are investigated using potentially practical examples of realizable structures in GaAs to illustrate the results.

Acknowledgments

This work was supported by the Air Force Office of Scientific Research under Grant No. AFOSR-81-0214.

References

1. See for example, A. Madhukar, J. Vac. Sci. Technol., 20, 149 (1982).

2. R. Dingle, H.L. Störmer, A.C. Gossard and W. Wiegmann, Surf. Sci. 98, 90 (1980).

3. J. Ihm, M. L. Cohen and S. F. Tuan, Phys. Rev. B, 23, 3258 (1981).

4. D. Pines and J. R. Schrieffer, Phys. Rev. 124, 1387 (1961).

5. J. Appel and A. W. Overhauser, Phys. Rev. B, 26, 507 (1982).

6. S. Dassarma and A. Madhukar, Phys. Rev. B, 23, 805 (1981).

7. J. C. Slater, Phys. Rev. 81, 385 (1951).

8. See for example C. Kittel, Quantum Theory of Solids, John Wiley & Sons, 1963, pp. 89.

Figure Captions

Fig. 1: Multilayered Heterostructure

(a) Configuration

(b) Conduction and Valence Band Edges

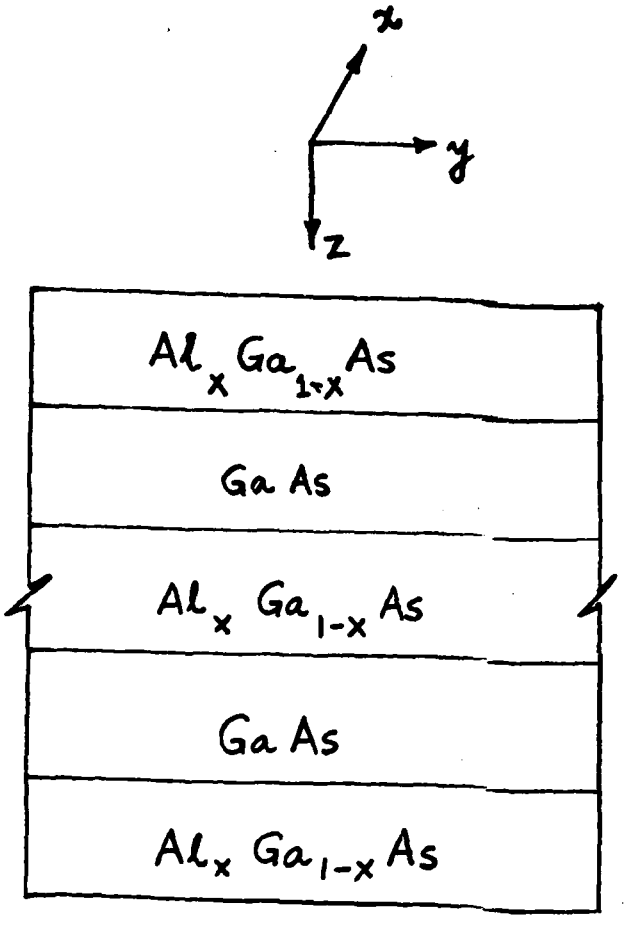

(a)

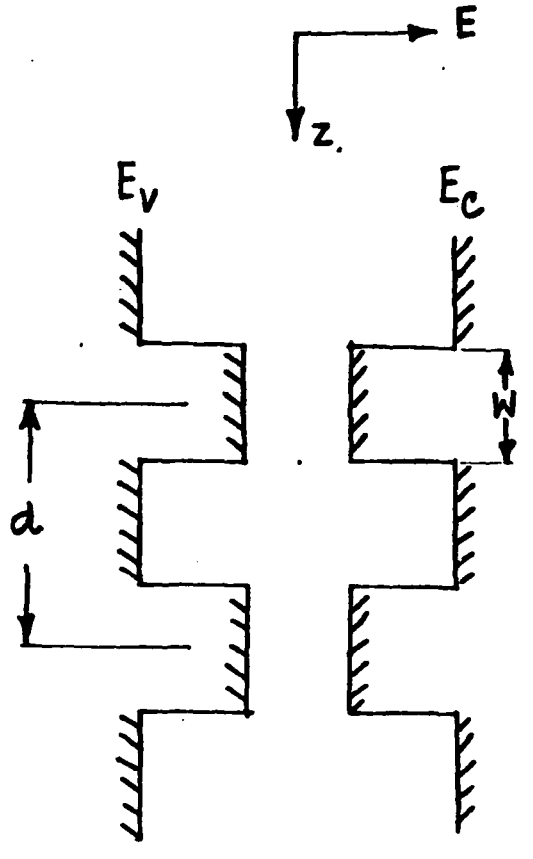

(b)

Fig. 1: Multilayered Heterostructure
(a) Configuration
(b) Conduction and Valence Band Edges


FILME
1-84